Deeply Virtual Meson Production on the nucleon

L. Favart[1], M. Guidal[2], T. Horn[3,4], P. Kroll[4]
[1]*IIHE - C.P. 230, Université Libre de Bruxelles*
1050 Brussels, Belgium
[2]*Institut de Physique Nucléaire d'Orsay*
CNRS-IN2P3, Université Paris-Saclay, 91406 Orsay, France.
[3]*Thomas Jefferson National Accelerator Facility*
Newport News, Virginia 23606, USA
[4]*The Catholic University of America*
Washington DC 20064, USA
[5]*Fachbereich Physik, Universität Wuppertal*
42097 Wuppertal, Germany.

June 21, 2016

arXiv:1511.04535v2 [hep-ph] 19 Jun 2016

Abstract

We review the status of the data and phenomenology in the Generalized Parton Distribution approach of Deep Virtual Meson Production.

1 Introduction

In recent years hard exclusive processes like deeply virtual photon (DVCS) and meson (DVMP) leptoproduction have attracted much interest. It has been shown that in the generalized Bjorken regime of large photon virtuality, Q^2, and large energy, W, in the virtual photon - proton center of mass frame, but fixed Bjorken-x, x_B, these processes factorize in hard partonic subprocesses and soft hadronic matrix elements parametrized as the generalized parton distributions (GPDs) [1, 2, 3, 4]. Fig. 1 illustrates this factorization for DVCS and DVMP. Rigorous proofs of factorization for DVMP are given in [5, 6]. In these references, it has also been shown that the asymptotically dominant contribution comes from longitudinally polarized photons while those arising from transversally polarized photons are suppressed by $1/Q^2$. It is not clear that there is such factorization for transversally polarized photons. For instance, in collinear approximation, the convolutions in the transverse amplitudes are infrared singular for light mesons. However, in phenomenologically studies, factorization of the latter amplitudes has been occasionally assumed to hold at least to leading-order of perturbation theory [7, 8, 9]. Factorization in hard subprocesses and GPDs has also been shown to hold to next-to-leading order (NLO) of perturbative QCD for photo- (and low Q^2) leptoproduction of Quarkonia in the formal limit of $m_Q \to \infty$ where m_Q is the mass of the heavy quark [10]. In photoproduction, the photons are transversally polarized. In low Q^2 leptoproduction of Quarkonia, longitudinal photons contribute, but the photon polarization is still predominantly transverse.

DVMP is complementary to DVCS. The quantum numbers of the produced meson allow one to probe different flavor combinations and allow for disentangling the various flavor GPDs. DVMP also

provides a way to access transversity GPDs. However, the abundance of opportunities provided by the produced meson in DVMP comes with additional experimental and theoretical challenges. In contrast to DVCS, the leading-twist hard scattering subprocesses for DVMP contain the exchange of hard quarks and gluons, which are accompanied by the appearance of the strong coupling constant α_s, and a meson distribution amplitude, whose functional form is not completely understood to date. As we will further discuss below, currently available experimental DVMP data are not yet in the regime where the leading-twist applies and strong power corrections are needed for their interpretation.

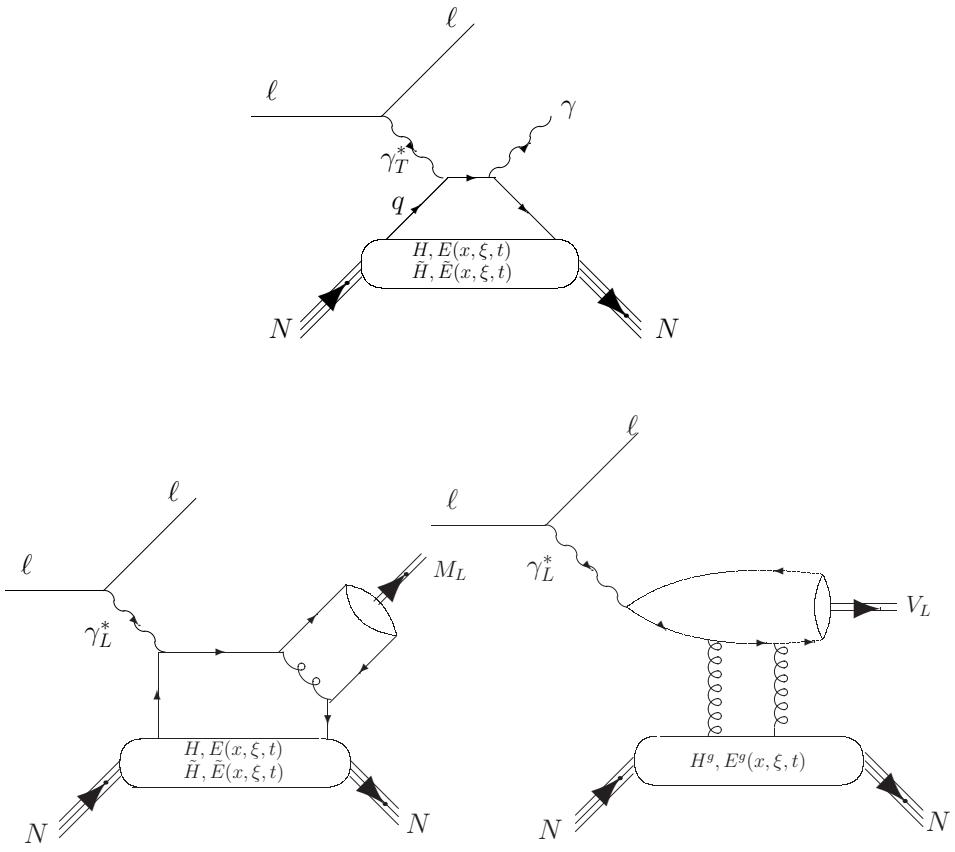

Figure 1: Top: a typical leading-twist DVCS handbag diagram. Bottom: typical leading-twist DVMP diagrams for the quark ($\gamma_L^* q \to M_L q$) and gluon ($\gamma_L^* g \to V_L g$) subprocesses. The symbol M stands for pseudo-scalar mesons as well as vector mesons while the symbol V stands only for vector mesons. The subscript L (T) stands for longitudinal (transverse) polarization.

The present article focuses on DVMP and aims at reviewing the status of the data and phenomenology in the field. We start by recalling some particular aspects of the handbag approach and the GPD phenomenology. For a detailed introduction to the theory of DVMP, we refer the reader to Refs.[11, 12] as well as to the introduction article devoted to GPDs and TMDs in this topical issue[13]. Then we will review the existing data for vector mesons and pseudoscalar mesons and discuss their current interpretation in terms of GPDs. We will conclude with a summary and the prospects for the field.

2 DVMP and GPDs

2.1 DVMP handbag amplitudes

The leading-twist DVMP amplitudes $\mathcal{M}$ are given by convolutions of the GPDs $K = K(x, \xi, t)$, where K is one of the leading-twist GPDs $H, E, \widetilde{H}, \widetilde{E}$ and the subprocess amplitudes, $\mathcal{H}$:

$$\begin{aligned}
\mathcal{M}^{M(q)}_{0+,0+} &= \frac{e_0}{2}\sqrt{1-\xi^2}\sum_q e_q \mathcal{C}^q_M \int_{-1}^{1} dx \sum_\lambda \mathcal{H}^{M(q)}_{0\lambda,0\lambda}\left[H^q_{\rm eff} + 2\lambda \widetilde{H}^q_{\rm eff}\right], \\
\mathcal{M}^{M(q)}_{0-,0+} &= \frac{e_0}{2}{\rm sgn}(\Delta^1)\frac{\sqrt{t_{\rm min}-t}}{2m}\sum_q e_q \mathcal{C}^q_M \int_{-1}^{1} dx \sum_\lambda \mathcal{H}^{M(q)}_{0\lambda,0\lambda}\left[E^q + 2\lambda\xi \widetilde{E}^q\right], \\
\mathcal{M}^{V(g)}_{0+,0+} &= \frac{e_0}{2}\sqrt{1-\xi^2}\sum_q e_q \mathcal{C}^q_V \int_{-1}^{1} dx \sum_\lambda \mathcal{H}^{V(g)}_{0\lambda,0\lambda}\, H^g_{\rm eff}\,, \\
\mathcal{M}^{V(g)}_{0-,0+} &= \frac{e_0}{2}{\rm sgn}(\Delta^1)\frac{\sqrt{t_{\rm min}-t}}{2m}\sum_q e_q \mathcal{C}^q_V \int_{-1}^{1} dx \sum_\lambda \mathcal{H}^{V(g)}_{0\lambda,0\lambda}\, E^g\,. \qquad (1)
\end{aligned}$$

Here, m denotes the mass of the proton and the skewness, ξ, is related to Bjorken-x, x_B, by $\xi = x_B/(2-x_B)$ up to corrections of order Q^2. Δ is the momentum transfer and $t = -\Delta^2$. Terms of order t/Q^2 are usually neglected. Forward scattering occurs at $t_{\rm min} = -4m^2\xi^2/(1-\xi^2)$. In Eq. 1, the indices of $\mathcal{M}$ refer to the helicities of the initial and final protons ($\pm$) and to the helicity of the initial photon and final meson (0's). The λ indices of $\mathcal{H}$ refer to the helicities of the partons participating to the subprocess. While the four GPDs $H, E, \widetilde{H}, \widetilde{E}$ are all helicity-conserving at the parton level, one sees that E and $\widetilde{E}$ contribute to the nucleon helicity-flip amplitudes and H and $\widetilde{H}$ to the nucleon helicity-conserving amplitudes. The symbols q refer to the quark flavors, g to gluons and "sgn" is the standard sign mathematical function. The non-zero flavor weight factors $\mathcal{C}$ are, for the electrically uncharged mesons like $\rho^0, \phi, \omega, \pi^0$:

$$\mathcal{C}^u_{\rho^0,\pi^0} = -\mathcal{C}^d_{\rho^0,\pi^0} = \mathcal{C}^u_\omega = \mathcal{C}^d_\omega = 1/\sqrt{2}, \quad \mathcal{C}^s_\phi = 1\,. \qquad (2)$$

The generalization to other mesons is straightforward [14].

Since the parton helicity, λ, is not observed it is to be summed over. The GPDs $H_{\rm eff}$ and $\widetilde{H}_{\rm eff}$ for quarks and gluons are the combinations

$$H_{\rm eff} = H - \frac{\xi^2}{1-\xi^2}E\,, \qquad \widetilde{H}_{\rm eff} = \widetilde{H} - \frac{\xi^2}{1-\xi^2}\widetilde{E}\,. \qquad (3)$$

The subprocess amplitudes, $\mathcal{H}$, for quarks and gluons, are to be calculated perturbatively from an appropriate set of Feynman graphs. Typical leading-order graphs for meson production are shown in the bottom two plots of Fig. 1. For the quark subprocess amplitude they lead to

$$\sum \mathcal{H}_{0\lambda,0\lambda} = \frac{32}{9Q}\pi\alpha_s(\mu_R) f_M \langle 1/\tau\rangle_M \left[\frac{1}{x-\xi+i\epsilon} + \frac{1}{x+\xi-i\epsilon}\right], \qquad (4)$$

where f_M and $\langle 1/\tau\rangle_M$ denotes the meson decay constant and the $1/\tau$-moment of its distribution amplitude, $\Phi_M(\tau)$; μ_R is an appropriate renormalization scale of order Q^2. Analogous expressions hold for the gluonic subprocess.

We note the model-independent feature that the leading-twist handbag approach predicts a $1/Q^6$ scaling of the longitudinal cross section, σ_L, for DVMP at fixed x_B which is modified by logarithms from the evolution and the running of α_S. The transverse cross section, σ_T, is expected to follow a $1/Q^8$ dependence at fixed Q^2 and x_B.

2.2 The parametrization of the GPDs

Since the GPDs are controlled by non-perturbative QCD there is no analytic method known for their calculation. Lattice QCD only allows for the calculation of the lowest few moments of the GPDs at unphysical values of the quark masses [15]. The extrapolation to the chiral limit is not fully understood [16, 17]. Thus, in order to learn about them one tries to extract them from suitable experimental observables like it is done for the parton density functions (PDFs). Such extractions require parametrizations which are frequently constructed from the double distribution representation of the GPDs [1, 18] assuming that the double distribution consists of a product of a zero-skewness GPD and a weight function:

$$\begin{aligned} K(x,\xi,t) &= \int_{-1}^{1} d\rho \int_{-1+|\rho|}^{1-|\rho|} d\eta\, \delta(\rho+\xi\eta-x)\, K(\rho,\xi=0,t) w(\rho,\eta) \\ &\quad + D(x/\xi,t)\, \Theta(\xi^2-x^2)\,. \end{aligned} \tag{5}$$

We refer the reader to Refs.[1, 18, 19] for the motivation to this approach. The GPDs constructed this way satisfy the polynomiality requirement, i.e. x-moments of the GPDs are polynomials in ξ. For H and E there is an additional D-term [20] which lives only in the region $-\xi < x < \xi$ as implied by the Heaviside function Θ. It provides a term $\sim \xi^{n+1}$ (for even n) to the n-th moment of these GPDs, while the integral term in Eq. (5) provides a polynomial in ξ only of order n. For (quarks) gluons the D-term is (anti)symmetric in the argument x/ξ and contributes with opposite sign to H and E. There is no D-term for the other GPDs. For valence quarks there is no D-term at all. According to the definition of the gluon GPDs there is an extra factor $|\xi|$ in front of the gluonic D-term.

For the weight function, w, that generates the skewness dependence, the form

$$w_(\rho,\eta) \;=\; \frac{\Gamma(2n+2)}{2^{2n+1}\Gamma^2(n+1)}\, \frac{[(1-|\rho|)^2-\eta^2]^n}{(1-|\rho|)^{2n+1}} \tag{6}$$

is often used, e.g. [7, 8, 21, 22]. The power n is regarded as a free parameter.

For the t-dependence, as the most simple ansatz for a zero-skewness GPD, one originally considered the product of its forward limit and a t-dependent form factor, e.g. $H^q(x,\xi=0,t) = q(\rho)F_1^q(t)$, [21]-[23]. Such an ansatz, factorizing in ρ and t, is evidently in conflict with Burkhardt's observation of a $\rho - t$ correlation [24, 25]. In later work a more complicated ansatz has been exploited

$$K(\rho,\xi=0,t) = k(\rho)\exp\left[f(\rho)t\right] \tag{7}$$

where $k(\rho)$ is either the appropriate parton distribution function (PDF) for H, $\widetilde{H}$ and H_T or, for the other GPDs, parametrized like the PDFs with some parameters to be adjusted to data: $N\rho^{-\alpha(0)}(1-\rho)^{\beta}$ (for gluon GPDs an extra power of ρ appears). The profile function, $f(\rho)$, is frequently parametrized in a Regge-like manner, e.g. [7, 8, 22, 26],

$$f(\rho) \;=\; B + \alpha' \ln(1/\rho)\,. \tag{8}$$

Since the function k behaves as $\sim \rho^{-\alpha(0)}$ at small ρ we have altogether a behavior as $\sim \rho^{-\alpha(t)}$ for the zero-skewness GPD with a linear Regge trajectory. Consider for example a typical Regge trajectory, $\alpha \simeq 0.5 + t$ GeV^{-2}. In this case the zero-skewness GPD behaves as $\sim 1/\sqrt{\rho}$ for $t \to 0$. For increasing $-t$ the singularity at $\rho = 0$ becomes milder and vanishes for $t \simeq -0.5$ GeV^2. This feature is to be contrasted with the results from the $\rho - t$ factorizing ansatz for which the zero-skewness GPD behaves as $\sim 1/\sqrt{\rho}$ for all t with strong consequences for the resulting GPD. This can be seen from Fig. 2 where the GPDs from the factorizing and from the Regge-like ansatz are compared to each other at $\xi = 0.1$ and $t = -0.5$ GeV^2. In both cases the same forward limit is used, i.e. the GPDs fall together at $t = 0$. With increasing $-t$ the GPDs differ in magnitude from each other more and more.

Although the Regge-like profile function possesses a $\rho - t$ correlation - small (large) $-t$ go along with small (large) ρ, it still has deficiencies at large ρ. To see this, we consider the GPD H for a quark flavor q as an example. The average impact parameter of $q(\rho, \mathbf{b})$, the Fourier transform of H^q with respect to the momentum transfer, at a given ρ, is [25]

$$\langle b^2 \rangle_\rho \;=\; \frac{\int d^2\mathbf{b}\mathbf{b}^2 q(\rho, \mathbf{b})}{\int d^2\mathbf{b} q(\rho, \mathbf{b})} \;=\; 4f(\rho) \tag{9}$$

In the proton's center of momentum the relative distance between the struck quark and the spectator system is $\mathbf{b}/(1-\rho)$. Its average

$$d(\rho) \;=\; \frac{\sqrt{\langle \mathbf{b}^2 \rangle_\rho}}{1-\rho} \tag{10}$$

can be regarded as an estimate of the size of the proton. For the profile function of Eq. (8) the distance d_q is singular for $\rho \to 1$. Because of this unphysical behavior the Regge-like ansatz cannot be used in the large ρ region.

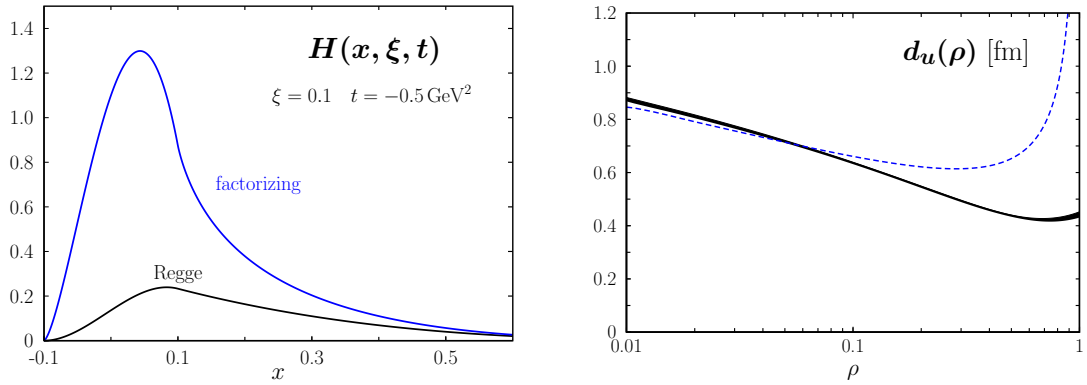

Figure 2: Left: A valence-type GPD constructed from the ρ-t factorizing and from the Regge-type double distribution at $\xi = 0.1$ and $t = -0.5$ GeV^2. The Regge trajectory is assumed to be $\alpha = 0.5 + t$ GeV^{-2}. Right: The average distance d_u for u-valence quarks. The solid line is the profile function of Eq. (11) with $A_u = 1.264$ GeV^{-2}, $B_u = 0.545$ GeV^{-2}, $\alpha' = 0.961$ GeV^{-2}; the dashed line was obtained from Eq. (8) with $B = 0$, $\alpha' = 0.9$ GeV^{-2}.

In order to cure this problem the following profile function has been advocated for in Refs. [27, 28] and utilized in an GPD analysis of the nucleon form factors:

$$f(\rho) \;=\; (B + \alpha' \ln(1/\rho))(1-\rho)^3 + A\rho(1-\rho)^2 \tag{11}$$

For this profile function the average distance between the struck quark and the cluster of spectators tends to the constant A for $\rho \to 1$, see Fig. 2. The first term of Eq. (11) dominates at low ρ and approximately falls together with the Regge-like profile function while at large ρ the second term becomes dominant. In Ref. [29] a profile function with just a $(1-\rho)^2$ term is discussed. The nucleon form factors are important constraints of the valence quark GPDs $H, E, \widetilde{H}$. The sum rules for the form factors allow to determine these GPDs at zero skewness for a given parametrization. For detailed analyses, see refs. [22, 27, 28]. Used as input to the double distribution representation of Eq. (5) the full valence quark GPDs can be evaluated and applied in analyses of hard exclusive reactions. Its application in deeply virtual meson production is discussed in the following sections.

An alternative parameterization of the GPDs starts from their double partial wave expansion in the conformal and in the t-channel SO(3) partial waves expansion [30]. However, this parametrization has been rarely used in actual analyses of DVMP. It goes without saying that all these ansätze hold at a low scale, typically a few GeV. The GPDs at larger scales are to be evaluated from the evolution equations. For instance, this can be achieved by using the Vinnikov code [31].

3 Review of Vector Mesons data and interpretation

3.1 Integrated cross section σ

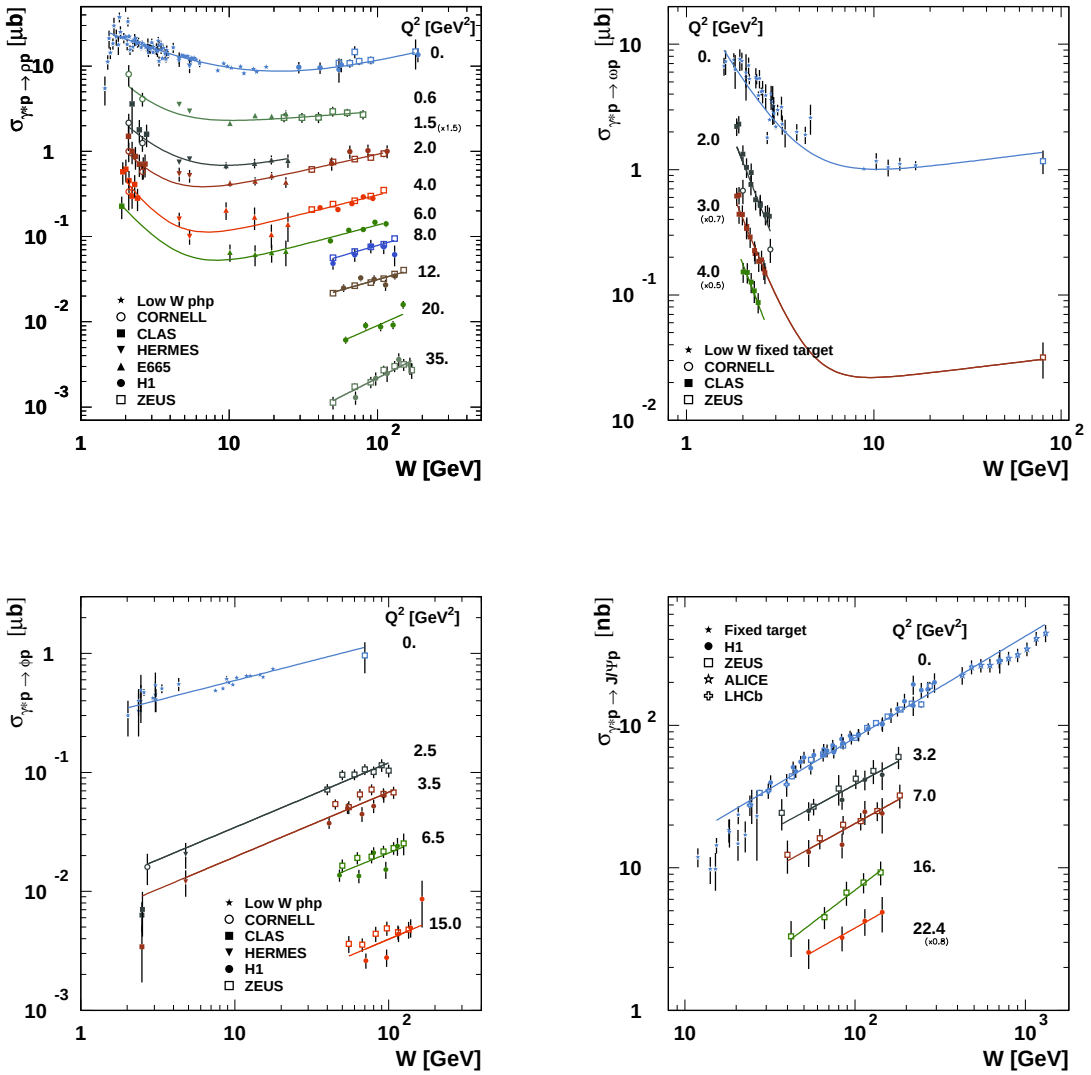

Figure 3: Top left: W-dependence of the $\gamma^{(*)}p \to p\rho^0$ cross sections for different Q^2 values ("php" denotes photoproduction). Some cross sections have been rescaled in Q^2 in order to compare between different experiments at the same Q^2. See text for data references. Top right: same for the ω channel. Bottom left: same for the ϕ channel. Bottom right: same for the J/Ψ channel. The curves indicate the results of the fit to the function of Eq. (12). The fits are done for W values large enough to be insensitive to threshold effects.

Due to a relatively high cross section, exclusive lepto- and photoproduction of vector meson on the proton is one of the exclusive processes the most studied experimentally. The cross sections for ρ^0, ω, ϕ, J/Ψ, $\Psi(2S)$, Υ production have been measured over a wide range of energies, from threshold up to $W \approx 200$ GeV for light mesons and, taking into account the recent LHC data, up to about 1 TeV for the heavy mesons. For light vector mesons, Q^2 ranges from Q^2=0 GeV^2 up to 100 GeV^2 in the high W

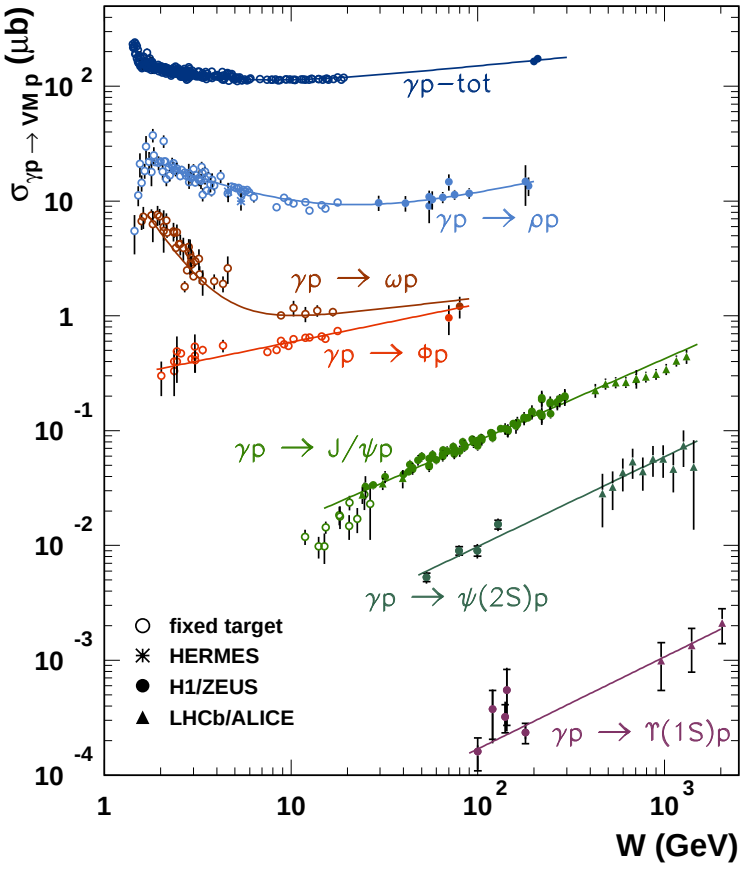

Figure 4: W-dependence of the photoproduction cross sections for the reactions $\gamma p \to p\rho^0, \omega, \phi, J/\Psi, \Psi(2S), \Upsilon$. The total γp cross section is also shown. The curves indicate the results of the fit to the function of Eq. (12).

domain, where there are data from the H1 [33, 34, 35], ZEUS [36, 37, 38, 39, 40, 41, 42] and HERMES[43] (HERA) and E665 (Fermilab)[44] experiments. At low W, experiments at CORNELL [45] and with the CLAS detector at Jefferson Lab [46, 47, 48, 49, 50] have measured the ρ^0, ω and ϕ electroproduction channels up to Q^2=5 GeV^2. For the heavy mesons, there are electroproduction data only for the J/Ψ from HERA [51, 54]; otherwise, there are photoproduction data coming from the H1 [52], ZEUS [53], LHCb [55, 56, 57, 58] and ALICE [59] experiments and a few fixed target data at low energies.

Fig. 3 shows representative data in leptoproduction, with some photoproduction data as well, and Fig. 4 shows all photoproduction data. For the ρ^0 and ω channels, two regimes are clearly apparent, in both lepto- and photoproduction. Starting from threshold, after a rapid rise due to the opening of the phase space, the cross sections decrease from $W \approx 2$ GeV down to $W \approx 7$ GeV. Then, the cross sections slowly rise with energy. For the other vector meson channels, ϕ, J/Ψ, $\Psi(2S)$ and Υ, above the threshold effect, there is only one behavior of the cross section: a steady rise with W from threshold up to the highest energies measured. One can clearly notice that the slope of the W-dependence at large W increases with Q^2 for the ρ^0 electroproduction channel and with the mass of the vector mesons for the photoproduction data. This indicates that the mass of the heavy mesons acts, like Q^2, as a hard scale.

In order to be quantitative, the cross section data in Figs. 3 and 4 have been fitted with the following function:

$$\sigma_V(W, \mu_V^2) = a_1 W^{\delta_1(\mu_V^2)} + a_2 W^{\delta_2(\mu_V^2)} \tag{12}$$

with a_1, a_2, δ_1 and δ_2 as free parameters. We define the scale μ_V^2 as $Q^2 + M_V^2$, where M_V is the mass of the vector meson, in correspondance with what we observed in Figs. 3 and 4. The light-meson mass is regarded as representative for the hadronic scale at which meson photoproduction occurs. In order to reduce the model dependence in the LHCb measured cross section as a function of W for the J/Ψ and $\Psi(2S)$ [55, 56, 58] to a negligible level with respect to the other systematics, only the high W solution discussed in Refs. [55, 56, 58] is kept in the fit. The curves in Fig. 3 and 4 show the results of these fits. Fig. 5 shows the dependence of δ_1 and δ_2 on μ_V^2. For the ϕ and the heavy mesons the parameter a_1 is zero. The power δ_1, characterizing the low energy behavior of the ρ^0 and ω cross sections, differs for these two reactions and increases in absolute value with increasing Q^2. To date, there is no theoretical explanation for δ_1. In contrast to the behavior of δ_1, the power δ_2 is approximately the same for the ρ^0 and ω cross sections as well as for the ϕ and heavy meson cross sections. This universal behavior of δ_2 will be explained below. It is, however, interesting to note that a recent article (Jones et al. [72]) analysed the J/Ψ and Υ photoproduction data including those from the LHC [55, 56, 57, 59]. The handbag amplitudes have been calculated to NLO accuracy [10]. It seems that the predictions for the J/Ψ cross sections underestimate the data, while good agreement with the Υ is found. According to [72], this indicates that the gluon density in recent PDF analysis is too small at low scales.

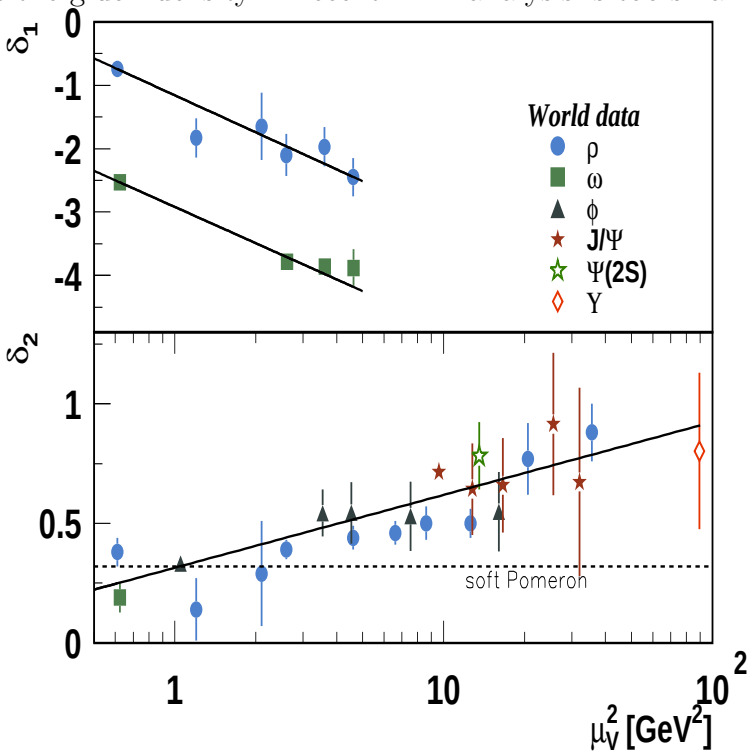

Figure 5: The Q^2-dependence of the powers δ_1 and δ_2 reflecting the W-dependence of the exclusive vector meson cross sections. The solid lines show fits of the form: $\delta(\mu_V^2) = A + B\ln(\mu_V^2)$ (μ_V^2 in GeV^2). For δ_2, one finds $A = 0.31 \pm 0.02$ and $B = 0.13 \pm 0.01$.

3.2 The longitudinal and transversal cross sections σ_L and σ_T

A feature to look at, in order to test the applicability of the handbag formalism, is whether the predicted dominance of the longitudinal part of the cross section can be observed experimentally. Most of the ρ^0 data of Fig. 3 have been L/T separated. Indeed, the analysis of the decay angular distribution of the

vector mesons gives access to the polarization states of the vector mesons. Then, assuming that the helicity between the final state vector meson and the initial virtual photon is conserved, one can deduce the polarization of the virtual photon, and thus σ_L and σ_T. This property is referred to as s-channel helicity conservation (SCHC). It can be checked experimentally by looking at specific decay matrix elements of the vector mesons [60] which are sensitive to $\gamma_L^* \to V_T$, $\gamma_T \to V_L$ or $\gamma_T^* \to V_{-T}$ transitions. SCHC has been found to hold sufficiently well for ρ^0 and ϕ production to allow for the L/T separation of the cross sections. Fig. 6 (left) presents the Q^2-dependence of the ratio σ_L/σ_T for ρ^0 production. It is predicted that this ratio should grow $\propto Q^2$ both as $Q^2 \to 0$ and, as predicted by the handbag approach, $Q^2 \to \infty$. This is realized at low Q^2 but the ratio is much milder than a $\propto Q^2$ behavior for $Q^2 \to \infty$. Though, taking into account parton transverse momenta, the handbag calculations[8, 9] can be put in agreement with the data. The cross section σ_L is larger than σ_T for $Q^2 \approx$1.5 GeV^2. The transverse cross section σ_T remains sizeable up to $Q^2 \approx 40$ GeV^2, the maximum Q^2 value at which it has been measured.

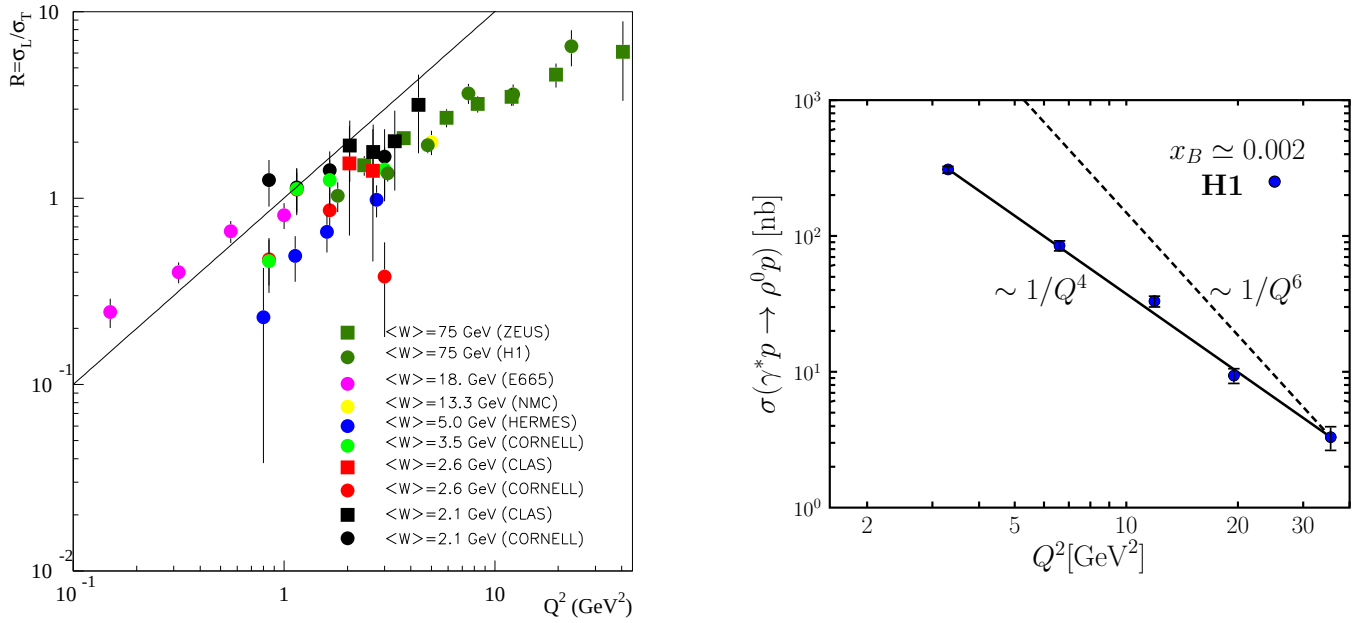

Figure 6: Left: The ratio σ_L/σ_T for ρ^0 leptoproduction versus Q^2. The solid line represents a $\propto Q^2$ dependence with arbitrary normalisation. Right: Measured Q^2-dependence of the ρ^0 cross section at fixed $x_B \approx$0.002. Data are from Refs. [46, 47] (CLAS), [45] (CORNELL), [43] (HERMES), [73] (NMC), [44] (E665), [33, 35] (H1) and [38] (ZEUS).

Another interesting feature to look at is the Q^2-dependence of the longitudinal cross section data. We recall that a prediction of the handbag approach is that the longitudinal cross section should scale, at fixed x_B, as $1/Q^6$ (up to evolution effects). In Fig. 6 (right), the H1 data for the ρ^0 cross section are shown at fixed $x_B \simeq 0.002$. The data span more than an order of magnitude in Q^2. One sees that the cross section falls approximately as $1/Q^4$, i.e. the Q^2 slope is milder than what is predicted by the leading-twist handbag formalism. Given the behavior of σ_L/σ_T, i.e. the σ_T contribution is all the more important as $Q^2 \to 0$, the experimental Q^2-dependence of σ_L is even flatter than $1/Q^4$. One may wonder whether higher-order perturbative corrections are responsible for this effect. As shown

by Diehl and Kugler [32], due to large BFKL-type logarithms, the NLO corrections to σ_L are huge at small skewness with opposite sign as compared to the LO term. A comparison with experiment however requires a resummation of these logarithms which has not yet been performed. An alternative concept is advocated for in [61]. In this work the GPD H, parametrized according to the double partial wave expansion and fitted to the HERA data on DVMP and DVCS to leading-twist accuracy, exhibit strong evolution effects. This means that the reduction of the $1/Q^6$ fall to an effective $1/Q^4$ one is realized by logarithms of Q^2. It remains to be seen whether this concept can be extended to smaller W. It should also be mentioned that a similar fit to only the DVCS data leads to different GPDs with much milder evolution effects.

In [62] it is suggested that the $\approx 1/Q^4$ behavior is generated by meson size effects modeled by quark transverse momentum in the subprocess while the emission and reabsorption of the partons from the proton are still treated in collinear approximation. The quark transverse momenta in the subprocess result in a separation of color sources in the impact parameter plane which is accompanied by gluon radiation. This is taken into account in [62] by a Sudakov form factor which includes the gluon radiation resummed to all orders of perturbation theory in next-to-leading-log approximation. Instead of distribution amplitudes $\mathbf{k}_\perp$-dependent light-cone wave functions have to be used with a parameter describing the transvere size of the meson. This approach turns into the leading-twist handbag result asymptotically. Its gluonic part bears resemblance to the color-dipole model [63, 71]. The approch has been generalized [8] in order to account also for transversally polarized photons. The infrared singularity appearing in collinear approximation in the corresponding amplitudes are regularized by the parton transverse momenta. The generalized handbag approach succesfully describes all ϕ and ρ^0 leptoproduction data, cross sections, spin density matrix elements and spin asymmetries for $W \geq 2$ GeV and ≥ 4 GeV, respectively. As an example, we show in Fig. 7 results from Ref. [8] and compare them to the HERA data. It is seen that it reproduces very well, in addition to the normalisation, the Q^2-dependence of σ_L and σ_T. In Fig. 8, we show the W-dependence of the longitudinal cross section for the ρ^0 and ϕ channels compared to this approach. There is a good agreement over the whole W-range for the ϕ-channel (for which there is only gluons exchange) but only for $W \gtrsim 4$ GeV for the ρ^0 channel.

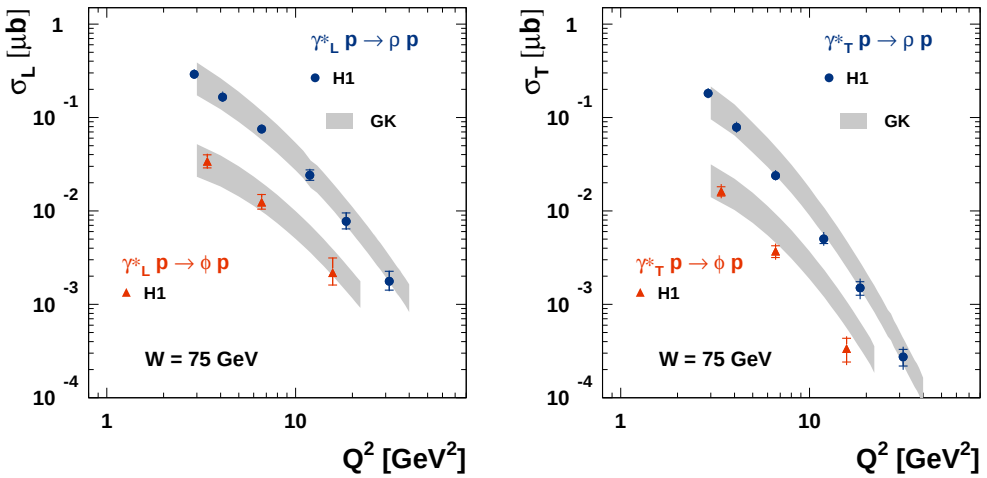

Figure 7: Left (right): comparison of the Q^2-dependence at fixed W=75 GeV with the GK model for σ_L (σ_T) of the ρ^0 and ϕ cross sections. The grey bands indicate the parametric uncertainties of the GK results [8]. Data are from Ref. [35] (H1).

At large energies and small x_B, the W-dependence of the cross sections shown in Figs. 3, 4 and 8

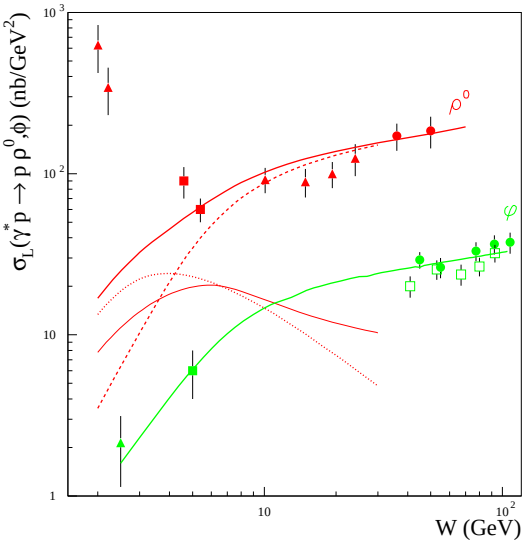

Figure 8: W-dependence at $Q^2 \approx 3.8$ GeV^2 of the $\gamma^* p \to p(\rho^0, \phi)$ cross sections in (red, green) compared to GK [8, 62] (thick solid curves) and VGG [21, 22] (red thin solid curve) calculations (the VGG calculation contains only quark exchange). The dashed (dotted) line represents the gluon plus sea (valence-quark plus (gluon + sea)-valence interference) contribution.

can be understood as follows: vector meson production in this kinematical region is a diffractive process with a dominantly imaginary amplitude which is fed by the gluonic GPD H^g. As can be seen from Eqs.(1) and (4), the imaginary part of the $\gamma^* p \to Vp$ amplitude is proportional to H^g for $x = \xi$:

$$Im\mathcal{M}^V_{0+,0+} \sim H^g(\xi,\xi,t)/\xi \tag{13}$$

From Eq.(5) one derives the small ξ behavior of the GPDs [64]

$$H^g(\xi,\xi,t) \;=\; c_g(\delta_g,\alpha'_g,n_g)2\xi g(2\xi)e^{t(B-\alpha'_g \ln(2\xi))} = c_g H^g(2\xi,0,t) \tag{14}$$

provided $xg(x) \sim x^{1-\delta_g(t)}$. The coefficent c_g is the skewing effect [65] which amounts to about 1.2 in the double-distribution ansatz. From Eq. (14) it follows that for small skewness and large W, the imaginary part of the scattering amplitude behaves as

$$Im\mathcal{M}^V_{0+,0+} \sim W^{2\alpha_g(t)} \tag{15}$$

with $\alpha_g = 1 + \delta_g + \alpha'_g t$. From analyticity of the scattering amplitude it follows that the real part has the same energy dependence for large W. Hence, the integrated cross section behaves as

$$\sigma_L \;=\; \int_{t_{\max}}^{t_{\min}} dt \frac{d\sigma}{dt} \sim W^{4(\alpha_g(t_{\min})-1)} \tag{16}$$

For HERA kinematics, $t_{\min}$ is approximately zero. Analogous results hold for the small ξ behavior of the quark GPDs. In the handbag approach advocated for in [8], the helicity amplitudes for transverse photons $M_{+\pm,+\pm}$ are also governed by H^g at large W and small skewness. Therefore, the above considerations and in particular Eq. (16) also hold for the transverse cross section of light vector-meson production. Since the production of Quarkonia is also under control of H^g [10], its cross section also follows Eq. (16). In Eq. (14) we see the close connection to the leading-log approximation invented by

Brodsky et al. [66] which is based on the gluon density. The difference to the handbag approach is the skewing effect c_g in Eq. (14). The sea quarks are usually neglected in applications of this model. Many variants of the leading-log approximation or color dipole model can be found in the literature. They mainly differ in the treatment of the subprocess $\gamma^* g \to V g$, see e.g. [63, 67, 68]. It is also been used in [21].

According to Eq. (16), for vector meson production at large W and small x_B the cross section behaves as $\sigma_L \sim W^{4\delta_g}$, where the power δ_g can be determined by experiment. The results of this determination are shown in the bottom panel of Fig 5 (note that $\delta_2 = 4\delta_g$) and compared to the soft Pomeron intercept [69]. We see that δ_g tends to a value below that of the soft Pomeron intercept of 0.08. Despite the large errors, δ_g seems to follow a universal behavior $\delta_g = A_g + B_g \ln(\mu_V^2)$ which we regard as a strong indication of a common underlying dynamical mechanism for light and heavy meson production. A realization of such a mechanism is the handbag approach with a dominant contribution from H^g. The increase of δ_g with Q^2 reflects the increase of the gluon density for $x \to 0$ due to the evolution. For light vector mesons, the situation is somewhat more complicated due to a substantial contribution from sea quarks [61, 62]. Due to quark-gluon mixing under evolution, the sea quarks, strictly speaking the flavor-singlet combination of quarks, is however expected to behave similar to the gluon and its contribution increases with approximately the same power of W as that of the gluons.

In the intermediate energy region, for W between 3 and 8 GeV, the valence quark GPDs become important, see Fig. 8. Their contributions have to be added coherently to the gluon and sea contributions resulting in interference effects. Since the valence-quark PDFs also behave as a power of x at low x with a power α_q that is smaller than α_g at small $-t$, it is obvious that the valence-quark contribution dies off quickly with increasing W at fixed Q^2. For low W, say below about 4 GeV, the cross section tends to increase strongly with decreasing W (see Fig. 3). This is reflected by the negative δ_1 values in Fig. 5. A similar strong increase is also seen for ω production but not for the ϕ channel. While the GK approach [62] works well for $W \gtrsim 4$ GeV it fails at smaller energies (Fig. 8). This is also the case for other handbag analyses [21, 70]. The discrepancy between theory and data is more than one order of magnitude in the low W region and the reason for this striking failure is not known today. One should note that for small W at fixed Q^2 skewness is large and consequently $-t_{\rm min}$ (for instance at $W = 2$ GeV and $Q^2 = 4$ GeV^2 $t_{\rm min} \simeq -0.9$ GeV^2). Thus, in this kinematical region the GPDs have to be extrapolated to rather large $-t$. Since the GPDs in the present parametrization with the Regge-like profile function of Eq. (8) are monotonously falling functions of $-t$ it is evident that the predicted cross section becomes small at low W at fixed Q^2.

3.3 Ratios of vector mesons cross sections

In search of signatures of the handbag mechanism, it is also instructive to look at the ratios of vector meson cross sections. In the large W/small skewness region, all vector meson channels are dominated by contributions from the gluon GPD H^g. Thus, up to wave function effects, the cross sections differ only by the charge content of the vector mesons. Hence, the ratio of cross section is predicted to be: $\sigma_{\rho^0}/\sigma_\omega/\sigma_\phi/\sigma_{J/\Psi} = 9/1/2/8$. In order to check these relations, we plot in Fig. 9, the ratios of the cross sections: $\sigma_V(W, Q^2)/\sigma_{\rho^0}(W, \mu_V^2)$, scaled by the corresponding charge ratio. Fig. 9 shows that the experimental cross section ratios are in good agreement with expectation for W of about 100 GeV. The data show a moderate dependence on Q^2. A possible explanation for this is that, in addition to the gluon contribution, there is a contribution from the quark sea (see Fig. 8). A flavor symmetric sea would also contribute according to the charge content. However at low scale the sea is not flavor symmetric. Strange and antistrange quarks are less abundant than the other light quarks. This effect leads to a mild logarithmic increase (from evolution) of the $\sigma_\phi/\sigma_{\rho^0}$ ratio. An analogous effect holds for the J/Ψ since charm quarks are strongly suppressed at low scales but contribute at large ones.

Turning to the energy domain of W=4 to 5 GeV, such as available at the HERMES experiment,

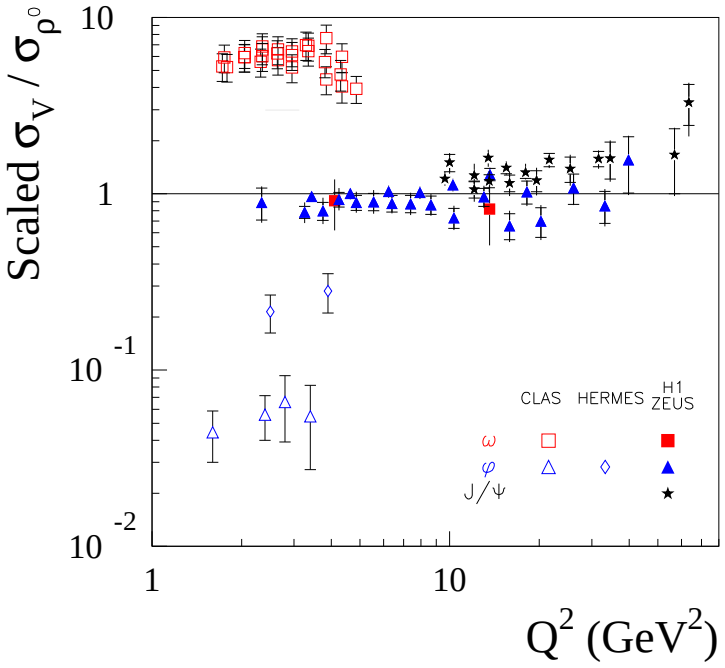

Figure 9: Ratio of the cross sections: $9 \times \sigma_\omega/\sigma_{\rho^0}$, $9/2 \times \sigma_\phi/\sigma_{\rho^0}$ and $9/8 \times \sigma_{J/\Psi}/\sigma_{\rho^0}$ as a function of Q^2 for different W's.

valence quarks of the proton also contribute to ρ^0 production, about 50% according to Fig. 8, but not to ϕ production. Thus, the ratio $\sigma_\phi/\sigma_{\rho^0}$ becomes very small as is seen in Fig. 9. For W between 2 and 4 GeV, characteristic of the CLAS experiment, the ρ^0 cross section becomes very large while the ϕ cross section continues to decrease so that the ratio $\sigma_\phi/\sigma_{\rho^0}$ gets smaller again. At these energies, the ω cross section is very close to the ρ^0 cross section (see Fig. 3) so that the ratio $9 \times \sigma_\omega/\sigma_{\rho^0}$ plotted in Fig. 9 is larger than one. Since the increase of the ρ^0 (and ω) cross section between W=2 and 4 GeV is not understood, it is not possible at this time to explain and predict the values of the cross section ratios at CLAS kinematics.

3.4 Slopes of differential cross section

Regarding the t-dependence of the cross sections, Fig. 10 shows the Q^2-dependence of the B parameter from the fit of the ρ^0 and J/Ψ differential cross section with the function Ae^{Bt}. One observes several features. The ρ^0 data at fixed Q^2 show an increase of B with increasing W. And, at fixed W, concentrating on the large W data (75 GeV), comparing the ρ^0 and J/Ψ Q^2-dependence, one can deduce a convergence of the B parameter for $Q^2 \approx 10$ GeV^2 around 4 GeV^{-2}.

As we already mentioned the high-energy J/Ψ photo- and leptoproduction amplitude is dominantly imaginary and under control of the GPD H^g at small skewness (for J/Ψ production, the skewness is given by $\xi = (M_{J/\Psi}^2 + Q^2)/(W^2 + Q^2)/2)$. As shown in [71], the slope parameter of the differential cross section is related to the average impact parameter of the gluon distribution at given $x = 2\xi$ by (see Eq. (9) with the quark distribution replaced by the corresponding gluon one):

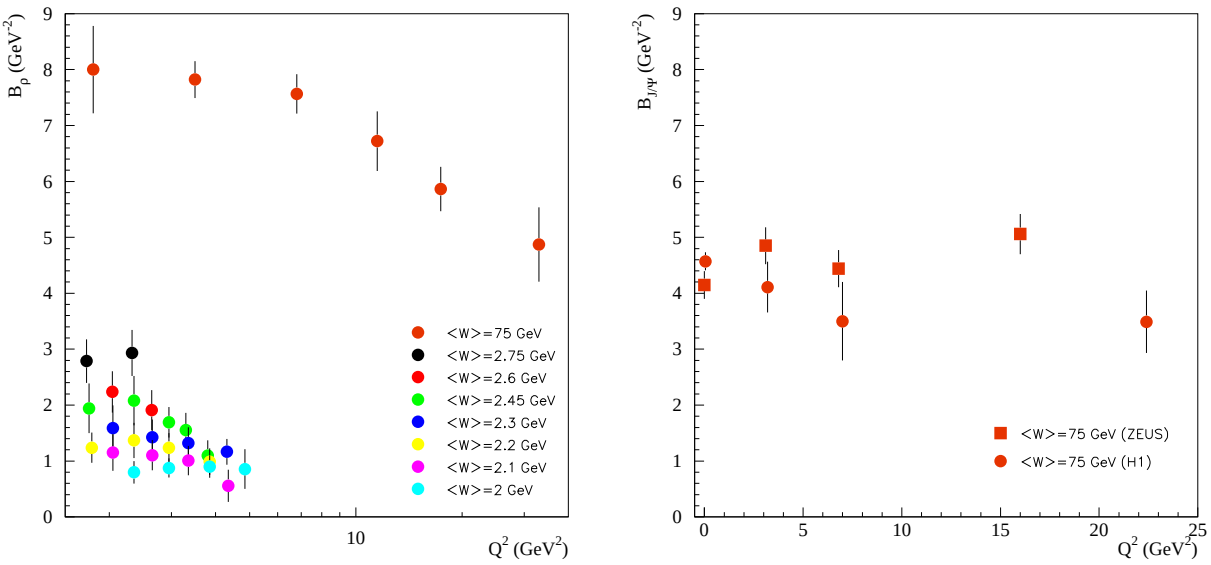

Figure 10: B-slope parameter as a function Q^2. Left: for the ρ^0, at different W's. Right: for the J/Ψ at W=75 GeV.

$$\langle b^2 \rangle^g_{x=2\xi} = \frac{\int d^2b b^2 g(x,b)}{\int d^2b g(x,b)} = 2B_{J/\Psi}\,. \tag{17}$$

In deriving this result one has to assume that $H^g(\xi,\xi,t)$ is proportional to $H^g(2\xi,0,t)$ which for instance is the case in the double-distribution parametrization (Eq. (14)). According to Eq. (10) and with regard to the fact that $x << 1$, $\langle b^2 \rangle^g_{x=2\xi}$ can be viewed as the transverse size of the nucleon's gluon distribution at $x = M^2_{J/\Psi}/W^2$. From the data shown in Fig. 10, one finds $d_g(2\xi) = \sqrt{\langle b^2 \rangle^g_{x=2\xi}} \simeq 0.55 - 0.63$ fm at $x \simeq 10^{-3}$ (at the scale $M^2_{J/\Psi}$) which is substantially smaller than the average size of the valence-quark distribution shown in Fig. 2 which holds at the scale 4 GeV^2. The gluonic size may increase logarithmically with decreasing x [71]. The interpretation of the ρ^0 slope parameter is more difficult. Quarks also contribute in addition to the gluon. For Q^2 larger than about 10 GeV^2 and high energies B^0_ρ approaches $B_{J/\Psi}$ indicating the increasing importance of the gluonic contribution.

4 Review of Pseudoscalar Mesons data and interpretation

4.1 The pion pole

The one-meson exchange plays an important role in leptoproduction of pseudo-scalar mesons. Its dominance in the longitudinal cross section is required for the extraction of the electromagnetic meson form factor from electroproduction data [74, 75]. As shown in Ref. [76] the pion pole contribution is also part of the GPD $\widetilde{E}$. Working out its contribution to the longitudinal cross section to leading-twist accuracy one finds,

$$\frac{d\sigma^{pole}}{dt}(\gamma^*_L \to \pi^+) = \frac{1}{\kappa}\frac{-t}{(t-m^2_\pi)^2} Q^2 \rho^2_{\pi\pi} \tag{18}$$

where $\rho_{\pi\pi}=\sqrt{2}e_0F_\pi(Q^2)g_{\pi NN}F_{\pi NN}(t)$, κ is a phase space factor, $F_{\pi NN}=\frac{\Lambda_N^2-m_\pi^2}{\Lambda_N^2-t}$ is the form factor that describes the t dependence of the pion-nucleon coupling, and $F_\pi(Q^2)$ is the perturbative contribution to the electromagnetic form factor of the pion. The latter amounts to only 30-50% of the experimental value of $F_\pi(Q^2)=\frac{1}{1+Q^2/\Lambda_\pi^2}$ (Λ_π^2=0.502 GeV^2) measured in the same process as we are discussing here. Using Eq. (18) with the perturbative form factor underestimates the cross section data by an order of magnitude at low $-t$. In Refs. [77, 78] it has therefore been suggested to use Eq. (18) with the experimental value of $F_\pi(Q^2)$, which is equivalent to evaluating the pion-pole contribution as an one-pion exchange term. Working out Eq. (18) in this way one obtains the results shown in Fig. 11. The bands indicate the calculated range of values for the parameters Λ_N=0.4-0.6 GeV and $g_{\pi NN}$=13.1-13.5.

Eq. (18) represents the pion pole contribution which is a special feature of the longitudinal pion electroproduction cross section. The pion pole includes a factor $-t/(t-m_\pi^2)^2$, which is zero at t=0 and reaches a maximum at t=$-m_\pi^2$. The first value is unphysical since forward scattering occurs at t_{min}=$-4m^2\xi^2/(1-\xi^2)$ while the second can be reached in experiments for $\xi \sim m_\pi/2m$. The value of the longitudinal π^+ cross sections in Fig. 11 is largest at small $-t$ <0.3 GeV^2 and falls off rapidly with increasing values of t. The data thus suggest a dominant pion pole in the longitudinal π^+ cross section at values of $-t$ <0.3 GeV^2. The dominance of the pion pole in the longitudinal cross section and its characteristic t dependence allows for extractions of the electromagnetic pion form factor from these data. The longitudinal cross section at W=2.2 GeV is in good agreement with the calculation of the pion pole contribution shown in Eq. (18). However, the pion pole calculation does not seem to describe the Q^2 dependence of the data very well at the lower value of W=1.95 GeV. The data at central values of Q^2=0.60, 0.75 (and 1.00) GeV^2 and W=1.95 GeV are systematically lower than the calculation. Adjusting the parametrization of the electromagnetic pion form factor to the data improves the overall agreement between data and calculation at the lower Q^2 settings, but does not provide an improvement of the overall description of the data set.

Unseparated π^+ data are available over a larger kinematic range in t and Q^2. It is thus interesting to see if one can use these data to obtain additional information on the importance of the pion pole, and if this information would have an impact on pion form factor extractions. Two extensive data sets on π^+ productions are available. One was obtained at HERMES [81] and another one with the CLAS at 6 GeV Jefferson Lab [82].

According to Fig. 12, Eq. (18) also describes the HERMES data at values of $-t$ <0.3 GeV^2. This implies that the monopole parametrization of the pion form factor with Λ_π based on pion form factor precision measurements approximately holds up to Q^2=5.4 GeV^2. At large $-t$ > 0.6 GeV^2, where one is farther away from the pion pole, the data deviate from the prediction by up to three sigma. The large role of the pion pole at small $-t$ < 0.3 GeV^2 in the unseparated π^+ cross section is interesting. However, this observation would not be sufficient to make a precise extraction of the electromagnetic pion form factor from the data. Without an explicit L/T separation it is not clear what fraction of the cross section is due to longitudinal photons and what the contribution of the pole to it is in these kinematics.

As an illustration of effects contributing at larger values of $-t$ Fig. 13 shows a comparison of the calculated pole contribution and the unseparated π^+ cross section data obtained with CLAS at Jefferson Lab 6 GeV at values of Q^2=2.35 GeV^2 and 3.85 GeV^2 and W of about 2.5 GeV. For values of $-t$ ∼0.3 GeV^2 the calculation underpredicts the data at similar values of Q^2 as compared to Fig. 12 suggesting a W dependence of other/non-pole contributions. Here, the tail of the pole contribution may also be competing with the background, which could be due to both longitudinal and transverse photons. To disentangle the longitudinal and transverse contributions a full separation of the cross section is needed. For a rough estimate of the transverse contribution one may compare the separated longitudinal and transverse cross sections from Fig. 11. There, the contribution of the transverse cross section can be up to 90% for $-t \sim 0.3$ GeV^2. Overall in the large $-t$ range, the calculated pion pole contribution is

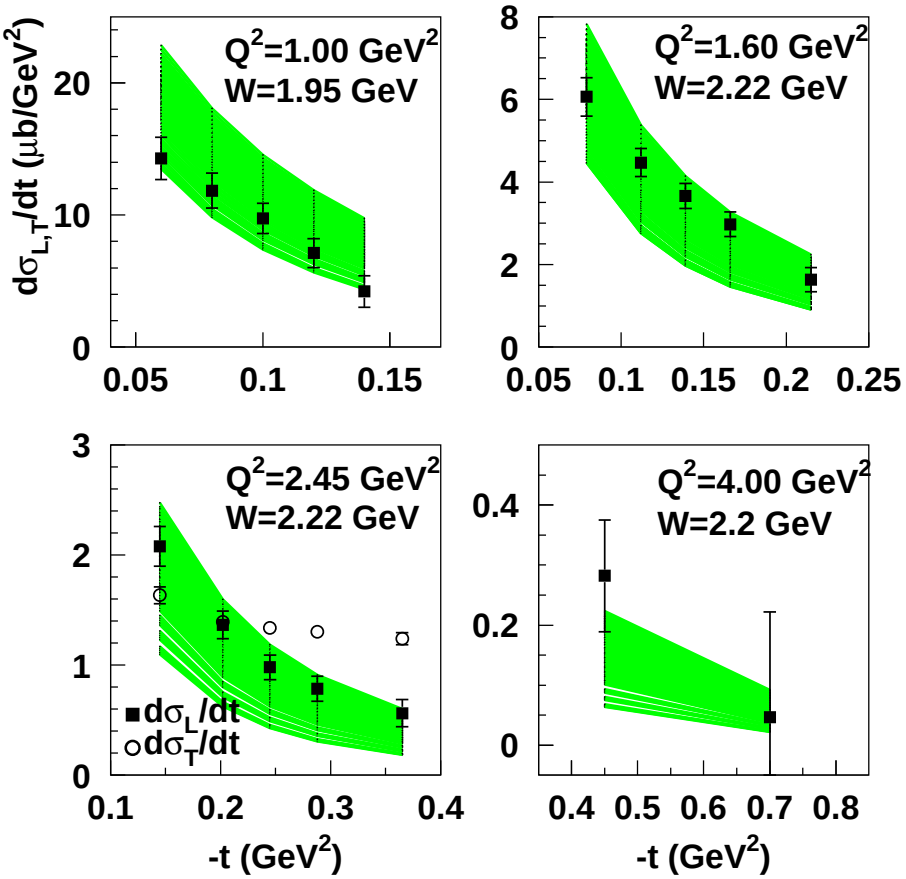

Figure 11: World precision π^+ electroproduction longitudinal cross sections at two values of W=2.2, 1.95 GeV and values of Q^2 ranging from 1.0 to 4.0 GeV^2. The data were obtained at 6 GeV Jefferson Lab using the focusing spectrometers in Hall C [79, 74, 80]. The green band indicates the calculated pole contributions according to Eq. (18) for a range of values of the parameters Λ_N=0.4-0.6 GeV and $g_{\pi NN}$=13.1-13.5. Note that the values of W and Q^2 listed in the figures are the overall central values. Each t bin has its own bin-centered W and Q^2 values.

systematically lower than the data at both Q^2 settings, which may be expected since the parametrization used in Eq. (18) is only reasonable near the pion pole.

To study the meson pole contribution as a function of the longitudinal momentum fraction x_B it is of interest to create a super set of data from different experiments at a fixed value of W and Q^2 and to analyze its dependence on t. Analyzing both kaons and pions in this way allows for a comparison of the relative importance of the pole in each channel. While the contribution of the meson pole in the longitudinal π^+ cross section has been shown to be dominant allowing for pion form factor extractions [75], its role in the longitudinal K^+ cross section at small values of t remains to be shown experimentally. Fig. 14 shows unseparated π^+ and K^+ cross sections binned in three bins of x_B and scaled to a common value of W=2.2 GeV and Q^2=1.6 GeV^2. The shaded areas denote the results of calculations of the meson pole contribution to the longitudinal cross section. For both the pion and the kaon pole calculation the formalism shown in Eq. (18) is used. The only changes in the calculation of the kaon pole contribution are the meson mass and the values of $g_{K\Lambda N}$ and Λ_N. The agreement of the calculation with the pion data seems to be as expected based on the results of the previous figures.

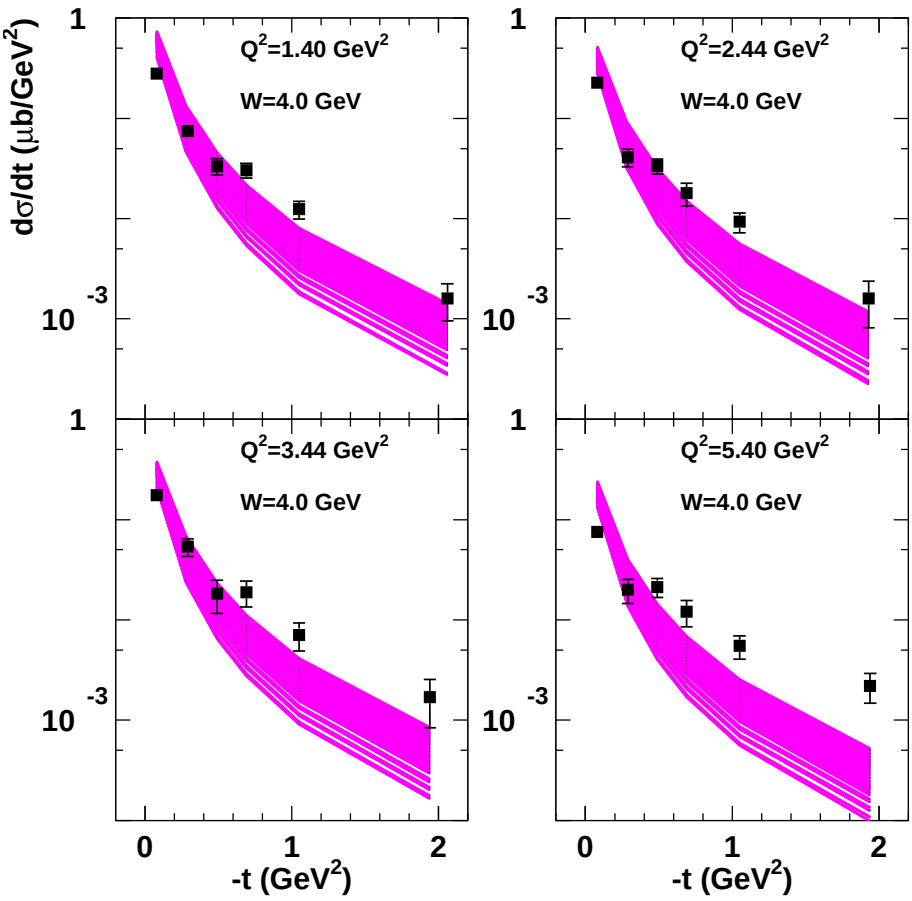

Figure 12: Unseparated π^+ electroproduction cross sections from HERMES. The bands shown are as in Fig.11.

There seems to be some small dependence on x_B. The kaon pole calculations underpredict the data by a factor of ∼100 for all x_B bins, which seems largely due to the larger kaon mass [83]. It should be noted that without the high energy and small angle capabilities offered by new facilities like the 12 GeV Jefferson Lab most of the K^+ data shown in Fig. 14 were obtained at relatively large values of $-t$ >0.3 GeV^2 and relatively small values of W <2 GeV. These data are always far away from the kaon pole, and thus its contribution to the longitudinal K^+ cross section is not dominant. However, a small maximum is expected in kaon production at small values of $-t$ [77, 78]. This needs to be verified experimentally. Measurements at the 12 GeV Jefferson Lab [84] at lower values of $-t$ are aimed at providing such data allowing for the interpretation of the kaon pole contribution. These data will provide a full separation of the kaon cross section is required allowing for an more detailed analysis of the role of the kaon pole and the relative contribution of longitudinal and transverse photons.

The relative contribution of longitudinal and transverse terms to the meson cross section and their t and Q^2 dependencies are of interest in evaluating the potential of probing the nucleon's transverse spatial structure through meson production. In general, only if experimental evidence for the leading-twist behavior can be shown one can be confident about a handbag formalism. One of the most stringent experimental tests is the Q^2 dependence of the longitudinal meson cross section. The measurement of the fully separated longitudinal and transverse contributions to the cross section at values of x_B experimentally accessible at, e.g., JLab 12 GeV, is essential for the interpretation of the data. Such

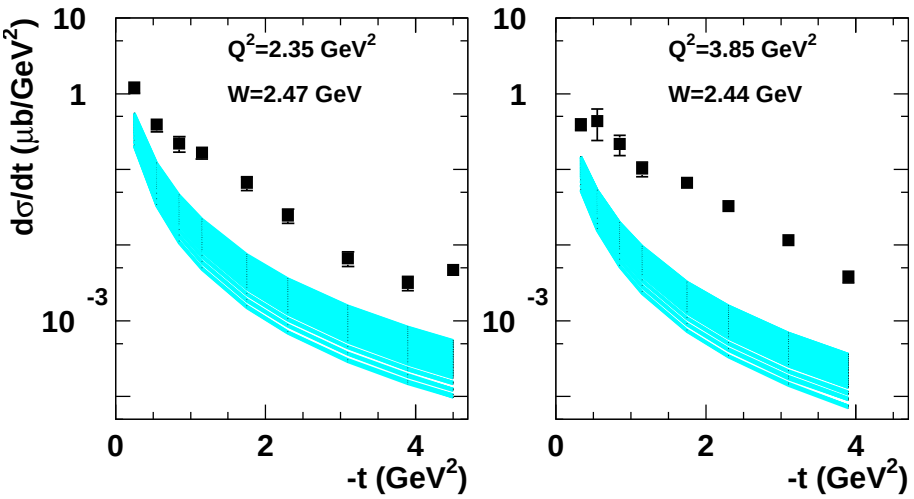

Figure 13: Unseparated π^+ electroproduction cross sections from 6 GeV JLab CLAS at values of W of 2.47 GeV and 2.44 GeV. The bands shown are as in Fig.11.

data are also needed for measurements of the exclusive pion form factor and its description as discussed in the beginning of this section. In the regime where the leading-twist formalism is applicable σ_L is predicted to scale as Q^{-6}, the transverse cross section is expected to scale as $\sigma_T \sim Q^{-8}$ and $\sigma_L >> \sigma_T$.

The leading-twist, lowest order calculation of the π^+ longitudinal cross section underpredicts the data by an order of magnitude. This implies that the data are not in the region where the leading-twist result applies. That current experimental data are not in the region where the leading-twist result applies can be seen in Fig. 15 showing the Q^2 and t dependence of the separated longitudinal and transverse π^+ cross sections. The QCD scaling prediction is fitted to, and indicated by, the solid black lines and is reasonably consistent with these data. It is clear σ_T does not follow the scaling expectation illustrated by the dashed black lines and the magnitude is large. Regarding the $-t$ dependence, Fig. 15 shows that $\sigma_L > \sigma_T$ for values of $-t < 0.3$ consistent with a dominant meson pole in this region and that $d\sigma_T > d\sigma_L$ for values of $-t > 0.3$ GeV^2 providing further evidence that the leading-twist does not apply in the currently available experimental kinematics.

The deviation of the π^+ cross sections from the leading-twist formalism may not be surprising. As discussed in section 3 for the vector meson ρ^0 production, the cross section can easily deviate from the anticipated Q^2 behavior in the scaling regime by power and logarithmic corrections. However, the measurements of the separated pseudoscalar meson cross sections and their dependencies are fundamental and important in their own right. Fully separated cross sections are essential for understanding dynamical effects in both Q^2 and $-t$ and interpretation of non-perturbative contributions in experimentally accessible kinematics. Such measurements of L-T separated cross sections will be enabled by the 12 GeV Jefferson Lab extending the current kinematic reach of π^+ data and including additional systems. These data will play an important role in our understanding of meson pole dominance and form factor extractions, and may provide experimental evidence allowing for interpretation of the data in the hand-bag formalism. In passing, we note that the pion pole also plays a prominent role in leptoproduction of omega mesons. In contrast to pion production the pole term contributes to the transverse amplitudes in this case [110].

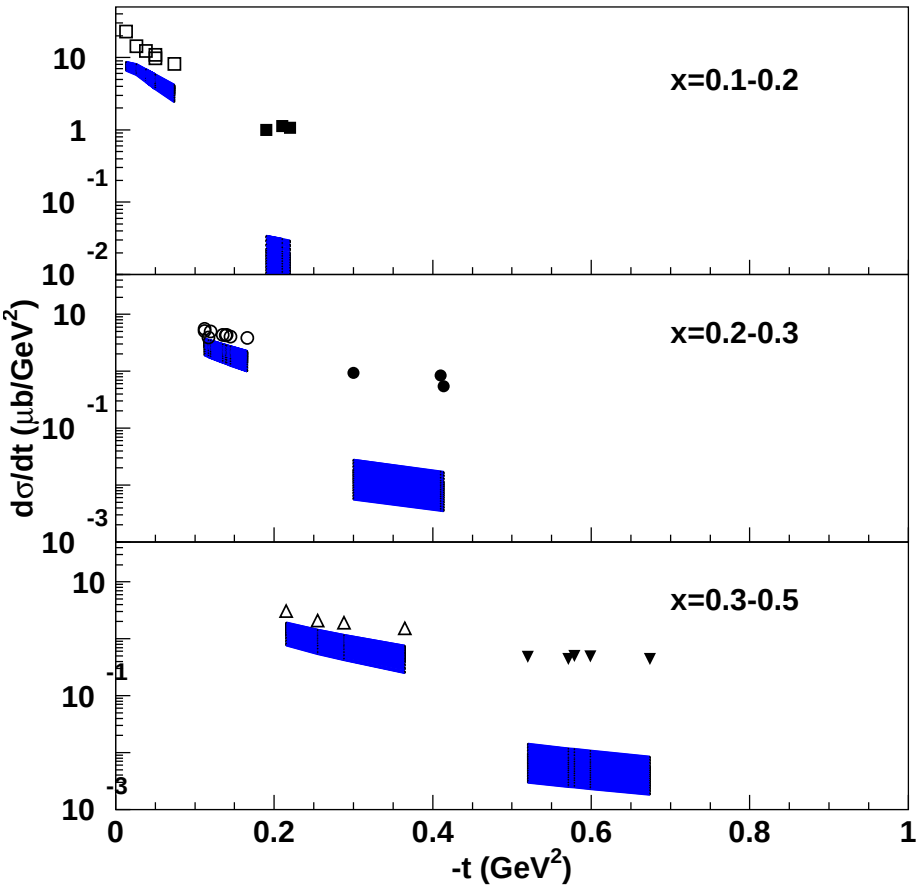

Figure 14: Unseparated pion and kaon electroproduction cross sections scaled to fixed values of Q^2=1.6 GeV^2 and W=2.2 GeV. World pion and kaon data include [81, 82, 79, 74, 80, 85, 86, 87, 88, 89, 90] and [91, 92, 93, 94, 95, 96, 97, 98, 99, 100, 101]. The open symbols denote exclusive π^+ and the filled symbols K^+ electroproduction data. Here, the data are binned in three x bins. The blue bands denote calculations of the pole contribution according to Eq. (18).

4.2 Transversity

Recent pion cross section data [74, 80, 102, 103, 104] suggest that transversely polarized photons play an important role in charged and neutral pion electroproduction. As shown in Fig. 11 L/T separated π^+ data show a large σ_T even at values of Q^2=2.5 GeV^2 and $-t$ <0.3 GeV^2. At HERMES a large $sin(\phi_S)$ modulation was observed in the Fourier amplitude or transverse target spin asymmetry, $A_{UT}(sin(\phi_s))$, which does not seem to vanish in the forward direction [102]. The observed behavior of the A_{UT} data demand a strong contribution from transverse photons. For $(t_{\rm min} - t) \rightarrow 0$ the only non-vanishing contribution to this observable is $Im(M^*_{0-,++}M_{0+0+})$. Thus, the transverse amplitude $M_{0-,++}$ must be of similar strength as the asymptotically leading longitudinal amplitude M_{0+0+} for π^+.

Fig. 16 shows separated charged [74, 79, 80] and unseparated neutral pion cross section data from 6 GeV Jefferson Lab [103]. For the charged pion data represented by the filled symbols in the upper panel the dominant role of the pole at values of $-t$ <0.3 GeV^2 is evident. Further one can see the characteristic fall off of σ_L as t increases resulting in σ_T to become larger than σ_L at values of $-t$ >0.3 GeV^2. The LT interference term in π^+ production is non-zero and positive while the TT interference term is negative and consistent with zero within the uncertainty over the region in t shown. This

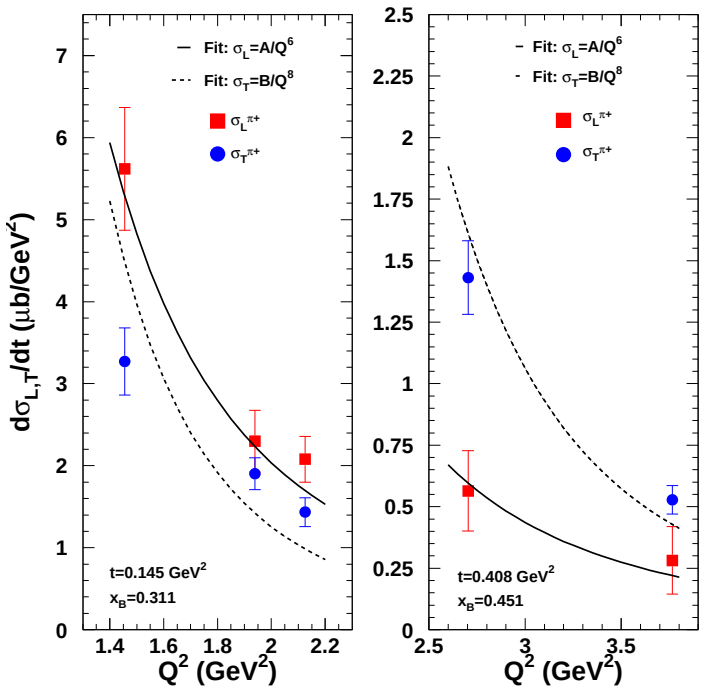

Figure 15: The longitudinal and transverse π^+ electroproduction cross sections at fixed values of x_B and $-t$. The solid line shows a fit to the σ_L of the form A/Q^6 and the dashed line a fit to σ_T of the form B/Q^8. The data are from Refs. [74, 79, 80]

behavior is consistent with that expected from angular momentum conservation shown in Fig. 17. The interference cross sections $d\sigma_{LT}$ and $d\sigma_{TT}$ vanish as $\sqrt{t_{\rm min}-t}$ and as $(t_{\rm min}-t)$ respectively. Thus, the interference cross sections become small for $t_{\rm min}-t \to 0$.

When looking at current neutral pion data as those presented in Fig. 16, it should be noted that these data are only available for values of $t \sim$0.2 GeV^2 and are not fully separated. The L-T interference term in π^0 production is small. In Fig. 16 it is negative on average, but it can also be positive depending on kinematics. In general, a non-zero L-T interference term would suggest that there is a longitudinal contribution to the cross section. The TT interference term in π^0 production is large in absolute value suggesting that transverse photons play an important role in this kinematic regime.

To interpret the data including a large contribution from transverse photons in Refs. [77, 78] the handbag approach is generalized to $\gamma_T^* \to M_L$ transition amplitudes. They are represented by convolutions of transversity GPDs and subprocess amplitudes calculated with a twist-3 pion wave function. The latter come along with a mass parameter μ_π which is given by the pion mass, m_π, enhanced by the chiral condensate

$$\mu_\pi = m_\pi^2/(m_u + m_d) \tag{19}$$

by means of the divergency of the axial vector current (m_u and m_d denote current quark masses). The transverse amplitudes are parametrically suppressed by μ_π/Q as compared to the asymptotically leading longitudinal amplitudes. As we mentioned in the first section, collinear factorization does not hold for the transverse amplitudes. However, if one allows for quark transverse momenta in the subprocess the infrared singularities disappear and $k_\perp$-factorization for the transverse amplitudes may hold.

As shown in Refs. [77, 78] the dominant transversity contributions at least at small $-t$ and small

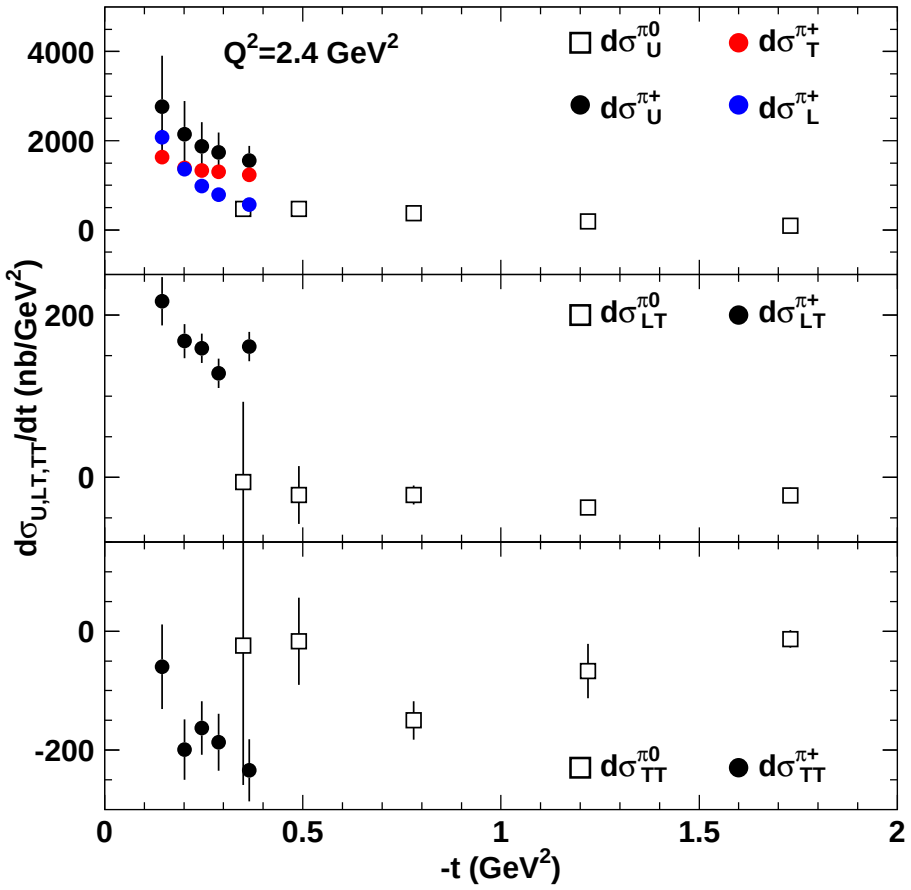

Figure 16: The L-T and T-T interference and unseparated pion cross sections (separated for π^+) at a value of Q^2=2.4 GeV^2 and $x_B \sim 0.4$. The data are from Refs. [74, 75, 103].

skewness are

$$\mathcal{M}_{0-,++} = e_0\sqrt{1-\xi^2}\int dx \mathcal{H}_{0-,++}H_T \tag{20}$$

$$\mathcal{M}_{0+,\pm+} = -e_0\frac{\sqrt{t_{min}-t}}{4m}\int dx \mathcal{H}_{0-,++}\bar{E}_T\,. \tag{21}$$

Parametrizing the transversity GPDs according to this formalism the trends and magnitudes of the π^+ and the interference terms of the π^0 data from JLab and HERMES are well described. Transversity GPDs in pion electroproduction have also been discussed in [105, 106, 107].

To confirm the estimates of the contribution of transverse photons and the potential to access GPDs in meson production requires a full separation of the cross section. The trends discussed above depend on both Q^2 and t, and thus it is important to cover as large of a kinematic range as possible including the regime $-t$ <0.3 GeV^2. The first L/T separated π^0 cross sections were measured Hall A at Jefferson Lab 6 GeV and are under analysis. These data cover a range in Q^2 between 1.5 and 2 GeV^2 and x_B of 0.36. A larger kinematic coverage for both charged and neutral pion (and kaon) production can be achieved with approved experiments at 12 GeV Jefferson Lab [108, 109, 84]. If experimental evidence for the dominance of σ_T can be demonstrated to hold, one may use these data to probe transversity GPDs.

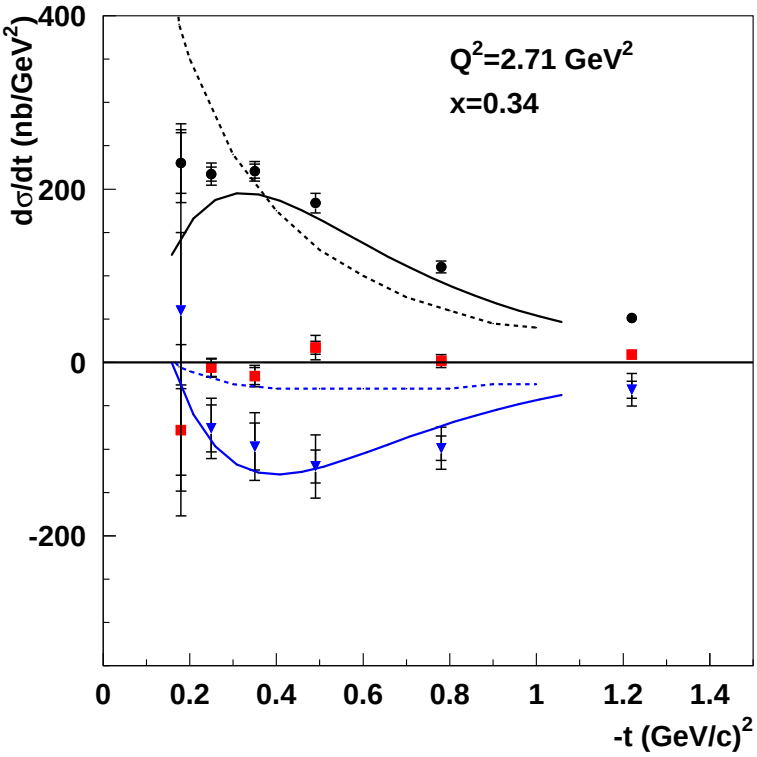

Figure 17: The L-T and T-T interference and unseparated pion cross sections at a value of Q^2=2.7 GeV^2 and $x_B \sim 0.4$ from Ref. [103] compared to the two theoretical predictions of Refs. [78] (solid) and [105, 106, 107] (dashed). Here, t_{min}=-0.15 GeV^2. The black symbols denote the unseparated cross section $\sigma_U=\sigma_T + \epsilon\sigma_L$, the blue symbols the T-T interference (σ_{TT}), and the red symbols the L-T interference (σ_{LT}). The inner error bars on the data points denote the statistical error and the outer error bars the statistical and systematic errors combined in quadrature.

5 Summary

Detailed inspection of the data on hard exclusive meson lepto- and photoproduction reveals clear evidence for a common dynamical mechanism underlying these processes for which the handbag approach is a serious candidate. However, most of the currently available experimental data are not in a region in which the leading-twist result applies. Only at very small values of x_B and Q^2 larger than about 50 GeV^2 do the data follow the leading-twist result. Nevertheless, detailed measurements of DVMP cross sections are important in order to understand dynamical effects and the interpretation of non-perturbative contributions in experimentally accessible kinematics. An example are the substantial contributions of transverse photons to the light meson channels, e.g., in neutral pion production. The dominance of transverse photons opens, if experimentally verified, new and unique opportunities for accessing the transversity GPDs over a large kinematic range.

On the theory front much progress has been made by including the contributions of transverse photons in light meson production into the handbag approach. This generalized handbag approach accounts for all observed features in the data with the exception of ρ^0 and ω production below values of $W < 4$ GeV.

Future measurements of DVMP cross sections will allow for confirming the estimates of transverse photon contributions and the potential to access GPDs in meson production, as well as to understand the remaining puzzles, e.g., the low W ρ^0 and ω cross section data. Such data are soon expected in the valence quark region with the 12 GeV upgraded JLab. With a beam energy of 11 GeV, a luminosity of 10^{35}cm^{-2}s^{-1} and 1000 hours of beam time with the CLAS12 detector for instance, about 100 million ρ^0 events are estimated to be collected (taking into account the CLAS12 acceptance). In particular, x_B values from <0.1 up to 0.8 and Q^2 values up to 12 GeV^2 can be reached, with L/T separation over most of the phase space for vector mesons.

These measurements of the vector meson cross sections in a large-acceptance setup will go hand-in-hand with precision pseudoscalar meson cross section measurements in Hall C. The heavily-shielded detector setup in a highly-focusing magnetic spectrometer with large momentum reach, rigid connection to a sturdy pivot, well-reproducible magnetic properties, and access to the highest-luminosity data (10^{38}cm^{-2}s^{-1}), provide the essential factors for meaningful longitudinal-transverse cross section separations. The anticipated excellent resolution and systematic understanding (less than 2% point-to-point) of the HMS-SHMS spectrometer pair best address the experimental requirements for this program.

Beyond the opportunities for DVMP studies in the kinematic region of the valence quarks afforded by the 12 GeV upgrade of CEBAF at JLab, the planned Electron-Ion Collider (EIC) will allow for exploring the role of the gluons and sea quarks in determining the hadron structure and properties. For example, measurements of Compton scattering as well as exclusive ρ^0 and J/Ψ production at high Q^2 could allow one to disentangle the singlet quark and gluon GPDs, and test the QCD evolution. The EIC also provides the facilities for measurements of two mesons with a large rapidity gap between them, which could be another interesting avenue to probe the GPDs for transversally polarized quarks. Further details on the EIC and its science can be found in Chapter "TMD and GPDs at EIC" in this review or Refs. [111, 112].

Acknowledgments

We are very thankful to A. Borissov, S. Goloskokov, X. Janssen, R. McNulty for the help they kindly provided. L. F. is supported by the "Fonds de la Recherche Scientifique -FNRS" of Belgium. M.G. benefitted from the ANR-12-MONU-0008-01 "PARTONS" contract support. T. H. is supported in part by NSF grant PHY-1306227.

References

[1] D. Mueller, D. Robaschik, B. Geyer, F. M. Dittes and J. Horejsi Fortsch. Phys. **42**, 101 (1994).

[2] X. -D. Ji, Phys. Rev. D **55**, 7114 (1997).

[3] A. V. Radyushkin, Phys. Lett. B **380**, 417 (1996).

[4] A. V. Radyushkin, Phys. Lett. B **385**, 333 (1996).

[5] J. C. Collins, L. Frankfurt and M. Strikman, Phys. Rev. D **56**, 2982 (1997).

[6] J. C. Collins and A. Freund, Phys. Rev. D **59**, 074009 (1999).

[7] S. V. Goloskokov and P. Kroll, Eur. Phys. J. C **42**, 281 (2005).

[8] S. V. Goloskokov and P. Kroll, Eur. Phys. J. C **53**, 367 (2008).

[9] A. D. Martin, M. G. Ryskin and T. Teubner, Phys. Rev. D **62**, 014022 (2000).

[10] D. Y. Ivanov, A. Schafer, L. Szymanowski and G. Krasnikov, Eur. Phys. J. C **34**, no. 3, 297 (2004); Eur. Phys. J. C **75**, no. 2, 75 (2015).

[11] M. Diehl, Phys. Rept. **388**, 41 (2003).

[12] A. V. Belitsky and A. V. Radyushkin, Phys. Rept. **418**, 1 (2005).

[13] M. Diehl, Eur. Phys. J. A **52**, 149 (2016).

[14] L. L. Frankfurt, P. V. Pobylitsa, M. V. Polyakov and M. Strikman, Phys. Rev. D **60**, 014010 (1999).

[15] P. Hägler, Phys. Rept. **490**, 49 (2010).

[16] G. S. Bali, S. Collins, M. Deka, B. Glassle, M. Gockeler, J. Najjar, A. Nobile and D. Pleiter *et al.*, Phys. Rev. D **86**, 054504 (2012).

[17] J. R. Green, M. Engelhardt, S. Krieg, J. W. Negele, A. V. Pochinsky and S. N. Syritsyn, Phys. Lett. B **734**, 290 (2014).

[18] A. V. Radyushkin, Phys. Lett. B **449**, 81 (1999).

[19] I. V. Musatov and A. V. Radyushkin, Phys. Rev. D **61**, 074027 (2000).

[20] M. V. Polyakov and C. Weiss, Phys. Rev. D **60**, 114017 (1999).

[21] M. Vanderhaeghen, P. A. M. Guichon and M. Guidal, Phys. Rev. D **60**, 094017 (1999).

[22] M. Guidal, M. V. Polyakov, A. V. Radyushkin and M. Vanderhaeghen, Phys. Rev. D **72**, 054013 (2005).

[23] M. Diehl, W. Kugler, A. Schafer and C. Weiss, Phys. Rev. D **72**, 034034 (2005) [Erratum-ibid. D **72**, 059902 (2005)].

[24] M. Burkardt, Phys. Rev. D **62**, 071503 (2000) [Erratum-ibid. D **66**, 119903 (2002)].

[25] M. Burkardt, Int. J. Mod. Phys. A **18**, 173 (2003).

[26] K. Goeke, M. V. Polyakov and M. Vanderhaeghen, Prog. Part. Nucl. Phys. **47**, 401 (2001).

[27] M. Diehl, T. Feldmann, R. Jakob and P. Kroll, Eur. Phys. J. C **39**, 1 (2005).

[28] M. Diehl and P. Kroll, Eur. Phys. J. C **73**, 2397 (2013).

[29] O. V. Selyugin and O. V. Teryaev, Phys. Rev. D **79**, 033003 (2009).

[30] D. Müller, M. V. Polyakov and K. M. Semenov-Tian-Shansky, JHEP **1503**, 052 (2015).

[31] A. V. Vinnikov, hep-ph/0604248.

[32] M. Diehl and W. Kugler, Eur. Phys. J. C **52**, 933 (2007).

[33] S. Aid *et al.* [H1 Collaboration], Nucl. Phys. B **463**, 3 (1996).

[34] C. Adloff *et al.* [H1 Collaboration], Eur. Phys. J. C **13**, 371 (2000).

[35] F. D. Aaron *et al.* [H1 Collaboration], JHEP **1005**, 032 (2010).

[36] J. Breitweg *et al.* [ZEUS Collaboration], Eur. Phys. J. C **2**, 247 (1998).

[37] J. Breitweg *et al.* [ZEUS Collaboration], Eur. Phys. J. C **6**, 603 (1999).

[38] S. Chekanov *et al.* [ZEUS Collaboration], PMC Phys. A **1**, 6 (2007).

[39] M. Derrick *et al.* [ZEUS Collaboration], Z. Phys. C **73**, 73 (1996).

[40] J. Breitweg *et al.* [ZEUS Collaboration], Phys. Lett. B **487**, 273 (2000).

[41] M. Derrick *et al.* [ZEUS Collaboration], Phys. Lett. B **377**, 259 (1996).

[42] S. Chekanov *et al.* [ZEUS Collaboration], Nucl. Phys. B **718**, 3 (2005).

[43] A. Airapetian *et al.*, Eur. Phys. J. C **17**, 389 (2000).

[44] M. R. Adams *et al.*, Z. Phys. C **74**, 237 (1997).

[45] D. G. Cassel, L. A. Ahrens, K. Berkelman, C. T. Day, B. G. Gibbard, D. J. Harding, D. L. Hartill and J. W. Humphrey *et al.*, Phys. Rev. D **24**, 2787 (1981).

[46] C. Hadjidakis et al., Phys. Lett. B **605**, 256 (2005).

[47] S. A. Morrow *et al.* [CLAS Collaboration], Eur. Phys. J. A **39**, 5 (2009).

[48] L. Morand et al., Eur. Phys. J. A **24**, 445 (2005).

[49] K. Lukashin et al., Phys. Rev. C **63**, 065205 (2001).

[50] J. Santoro et al., Phys. Rev. C **78**, 025210 (2008).

[51] A. Aktas *et al.* [H1 Collaboration], Eur. Phys. J. C **46**, 585 (2006).

[52] C. Alexa *et al.* [H1 Collaboration], Eur. Phys. J. C **73**, 2466 (2013).

[53] S. Chekanov *et al.* [ZEUS Collaboration], Eur. Phys. J. C **24**, 345 (2002).

[54] S. Chekanov *et al.* [ZEUS Collaboration], Nucl. Phys. B **695**, 3 (2004).

[55] R. Aaij *et al.* [LHCb Collaboration], J. Phys. G **40**, 045001 (2013).

[56] R. Aaij *et al.* [LHCb Collaboration], J. Phys. G **41**, 055002 (2014).

[57] R. Aaij *et al.* [LHCb Collaboration], JHEP **1509**, 084 (2015).

[58] R. McNulty [for the LHCb Collaboration], arXiv:1511.07302 [hep-ex].

[59] B. B. Abelev *et al.* [ALICE Collaboration], Phys. Rev. Lett. **113**, no. 23, 232504 (2014).

[60] K. Schilling and G. Wolf, Nucl. Phys. B **61** (1973) 381.

[61] M. Meskauskas and D. Müller, Eur. Phys. J. C **74**, no. 2, 2719 (2014).

[62] S. V. Goloskokov and P. Kroll, Eur. Phys. J. C **50**, 829 (2007).

[63] J. Nemchik, N. N. Nikolaev, E. Predazzi and B. G. Zakharov, Z. Phys. C **75**, 71 (1997).

[64] P. Kroll, EPJ Web Conf. **85**, 01005 (2015).

[65] A. D. Martin and M. G. Ryskin, Phys. Rev. D **57**, 6692 (1998).

[66] S. J. Brodsky, L. Frankfurt, J. F. Gunion, A. H. Mueller and M. Strikman, Phys. Rev. D **50**, 3134 (1994).

[67] L. Frankfurt, W. Koepf and M. Strikman, Phys. Rev. D **54**, 3194 (1996).

[68] D. Y. Ivanov and R. Kirschner, Phys. Rev. D **58**, 114026 (1998).

[69] A. Donnachie and P. V. Landshoff, Phys. Lett. B **478**, 146 (2000).

[70] K. Kumericki, T. Lautenschlager, D. Mueller, K. Passek-Kumericki, A. Schaefer and M. Meskauskas, arXiv:1105.0899 [hep-ph].

[71] M. Strikman and C. Weiss, Phys. Rev. D **80**, 114029 (2009).

[72] S. P. Jones, A. D. Martin, M. G. Ryskin and T. Teubner, arXiv:1507.06942 [hep-ph].

[73] M. Arneodo *et al.* [NMC Collaboration], Nucl. Phys. B **429**, 503 (1994).

[74] T. Horn et al., Phys. Rev. Lett. **97**, 192001 (2006).

[75] H. P. Blok et al., Phys. Rev. C **78**, 045202 (2008).

[76] L. Mankiewicz, G. Piller, A. Radyushkin, Eur. Phys. J. **C10**, 307 (1999).

[77] S. V. Goloskokov and P. Kroll, Eur. Phys. J. C **65**, 137 (2010)

[78] S. V. Goloskokov and P. Kroll, Eur. Phys. J. A **47**, 112 (2011)

[79] V. Tadevosyan et al., Phys. Rev. C **75**, 055205 (2007).

[80] T. Horn et al., Phys. Rev. C **78**, 058201 (2008).

[81] A. Airapetian et al., Phys. Lett. **B659**, 486 (2008).

[82] K. Park et al., Europ. Phys. J. **A49**, 16 (2013).

[83] T. Horn, Phys. Rev. C **85**, 018202 (2012).

[84] T. Horn, G. Huber et al., Approved Jefferson Lab experiment E12-09-011. http://www.jlab.org/exp_prog/proposals/09/PR12-09-011.pdf

[85] C. N. Brown et al., Phys. Rev. Lett. **26**, 987 (1971).

[86] C. N. Brown et al., Phys. Rev. Rev. **D8**, 92 (1973).

[87] C. J. Bebek et al., Phys. Rev. D **13**, 25 (1976).

[88] C. J. Bebek et al., Phys. Rev. D **17**, 1693 (1978).

[89] P. Brauel et al., Phys. Lett. **B65**, 184 (1976); Phys. Lett. **B69**, 253 (1977).

[90] H. Ackermann et al., Nucl. Phys. **B137**, 294 (1978).

[91] C. N. Brown et al., Phys. Rev. Lett. **28**, 1086 (1972).

[92] C. J. Bebek et al., Phys. Rev. Lett. **37**, 1326 (1976).

[93] C. J. Bebek et al., Phys. Rev. D **15**, 594 (1977).

[94] T. Azemoon et al., Nucl. Phys. B **95**, 77 (1975).

[95] P. Brauel et al., Z. Phys. **C3**, 101 (1979).

[96] P. Ambrozewicz et al., Phys. Rev. C **75**, 045203 (2007).

[97] D.S. Carman et al., Phys. Rev. Lett. **90**, 131804 (2003).

[98] D.S. Carman et al., Phys. Rev. C **79**, 065205 (2009).

[99] D.S. Carman et al., Phys. Rev. C **87**, 025204 (2013).

[100] R. Mohring et al., Phys. Rev. C **67**, 055205 (2003).

[101] M. Coman et al., Phys. Rev. C **81**, 052201 (2010).

[102] A. Airapetian et al., Phys. Lett. B**682**, 345 (2010).

[103] I. Bedlinskiy et al., Phys. Rev. Lett. **109**, 112001 (2012).

[104] E. Fuchey et al., Phys. Rev. C **83**, 025201 (2011).

[105] S. Ahmad, G.R. Goldstein, S. Liuti, Phys. Rev. D **79**, 054014 (2009).

[106] G.R. Goldstein, J.O.G. Hernandez, S. Liuti, J. Phys. G: Nucl. Part. Phys. **39**, 115001 (2012).

[107] G.R. Goldstein, J.O.G. Hernandez, S. Liuti, Phys. Rev. D **91**, 114013 (2015).

[108] C. Muñoz-Camacho et al., Approved Jefferson Lab experiment E12-13-010. http://www.jlab.org/exp_prog/proposals/13/PR12-13-010.pdf

[109] T. Horn, G. Huber et al., Approved Jefferson Lab experiment E12-07-105. http://www.jlab.org/exp_prog/proposals/07/PR12-07-105.pdf

[110] S. V. Goloskokov and P. Kroll, Eur. Phys. J. A **50**, no. 9, 146 (2014).

[111] A. Accardi et al. Electron Ion Collider: The Next QCD Frontier - Understanding the glue that binds us all, BNL-98815-2012-JA, JLAB-PHY-12-1652, arXiv:1212.1701 (2012).

[112] DOE/NSF Nuclear Science Advisory Committee, "Reaching for the Horizon - The 2015 Long Range Plan for Nuclear Science", available online: http://science.energy.gov/~/media/np/nsac/pdf/2015LRP/2015_LRPNS_091815.pdf.